Endothelial-secreted Endocan protein acts as a PDGFR alpha ligand and regulates vascularity, radioresistance, and regional phenotype in glioblastoma

Soniya Bastola[1,4#], Marat S. Pavlyukov[1#], Yasmin Ghochani[1], Neel Sharma[1], Mayu A. Nakano[2], Sree Deepthi Muthukrishnan[1], Sang Yul Yu[1], Min Soo Kim[1,3], Alireza Sohrabi[4], Natalia P. Biscola[5], Daisuke Yamashita[6], Ksenia S. Anufrieva[7], Riki Kawaguchi[8], Yue Qin[8], Stephanie K. Seidlits[4], Alma L Burlingame[9], Juan A. Oses-Prieto[9], Leif A. Havton[10], Steven A. Goldman[11], Anita B. Hjelmeland[12], Ichiro Nakano[13,14*] and Harley I. Kornblum[1, 14*]

[1]The Intellectual and Developmental Disabilities Research Center, The Semel Institute for Neuroscience and Human Behavior, and The Broad Stem Cell Research Center, The Jonsson Comprehensive Cancer Center, David Geffen School of Medicine at UCLA, Los Angeles, CA 90095, USA
[2]Precision Medicine Institute, University of Alabama at Birmingham, AL 35294, USA
[3]Johns Hopkins University School of Medicine, Baltimore, MD 21205, USA
[4]Department of Bioengineering, University of California Los Angeles, Los Angeles, CA 90095 USA
[5]Department of Neurology, Icahn School of Medicine at Mount Sinai, New York, NY, 10029, USA
[6]Department of Neurosurgery, Ehime University Graduate School of Medicine, Shitsukawa 454, Toon, Ehime 791-0295, Japan
[7]Center for Precision Genome Editing and Genetic Technologies for Biomedicine, Federal Research and Clinical Center of Physical-Chemical Medicine of Federal Medical Biological Agency, Moscow, Russia; Moscow Institute of Physics and Technology, Moscow Region, Russia
[8]Interdepartmental Program in Bioinformatics, Program in Neurogenetics, Department of Neurology and Department of Human Genetics, David Geffen School of Medicine at UCLA, Semel Institute for Neuroscience and Human Behavior, Departments of Psychiatry and Neurology, David Geffen School of Medicine, University of California, Los Angeles, 695 Charles E Young Dr. South, Gonda Bldg, Rm 1524, Los Angeles, CA, 90095, USA
[9]Department of Pharmaceutical Chemistry, University of California, San Francisco, San Francisco CA 94158, USA
[10]Departments of Neurology and Neuroscience, Icahn School of Medicine at Mount Sinai, New York, NY 10029; James J Peters VA Medical Center, Bronx, NY 10468
[11]Center for Translational Neuromedicine, University of Rochester Medical Center, Rochester, NY, 14642, USA; and Faculty of Health and Medical Sciences, University of Copenhagen, Copenhagen 2200, Denmark
[12]Department of Cell, Developmental and Integrative Biology, University of Alabama at Birmingham, Birmingham, AL 35294 USA
[13]Department of Neurosurgery, Harada Hospital Address: 1-13-3 Toyooka, Iruma, Saitama 358-0003, Japan
[#] Co-first authorship

*[14] Corresponding authors/Correspondence:
Harley Kornblum, MD, PhD
hkornblum@mednet.ucla
Ichiro Nakano, MD, Ph.D.,
Dr.ichiro.nakano@gmail.com

Running Title: VE cells promote GBM aggressiveness via Endocan-PDGFRA signaling

Keywords: brain cancer; glioma; glioblastoma; Endocan; *Esm1*; PDGFRA; Myc; angiogenesis; endothelial cells; radioresistance

Conflict of interest disclosure statement: The authors declare no potential conflicts of interest.

Number of figures: 8 main figures, 7 supplemental figures

Abstract

One of the hallmarks of glioblastoma (GBM) is extensive neovascularization. In addition to supplying blood and nutrients, vascular endothelial (VE) cells provide trophic support to GBM cells via paracrine signaling, the precise mechanisms of which are being unraveled. Here, using patient-derived GBM and VE cells as well as orthotopic GBM mouse models, we report that Endocan (*ESM1*), an endothelial-secreted proteoglycan, confers enhanced proliferative, migratory, and angiogenic properties to GBM cells and regulates their spatial identity. Mechanistically, Endocan exerts at least part of its functions via direct binding and activation of the PDGFRA receptor. Subsequent downstream signaling enhances chromatin accessibility of the Myc promoter and upregulates Myc expression inducing highly stable phenotypic changes in GBM cells. Furthermore, Endocan confers a radioprotection phenotype in GBM cells, both *in vitro* and *in vivo*. Inhibition of Endocan-PDGFRA signaling with ponatinib increases survival in the *Esm1* wild-type but not in the *Esm1* knock-out mouse GBM model. Our findings identify Endocan and its downstream signaling axis as a potential target to subdue the recurrence of GBM and further highlight the importance of vascular to tumor cell signaling for GBM biology.

Significance statement

Identification of the Endocan/PDGFRA/Myc axis demonstrates an important role of VE cells in GBM malignancy. The contribution of Endocan to the development of GBM cell populations with different phenotypes reveal an additional pathway underlying the origin of GBM intratumoral heterogeneity. Targeting Endocan-mediated crosstalk may enhance the efficacy of GBM treatment.

Introduction

Glioblastoma (GBM) is a highly aggressive, vascular-rich tumor that exploits vascular endothelial (VE) cells to contribute to its growth[1,2]. VE cells provide paracrine factors, nutrition, oxygen, as well as a niche for glioma stem cells (GSCs)[1,3,4]. GSCs residing within the perivascular niche maintain the capacity for self-renewal and promote GBM progression, and recurrence[3,5]. Developing an understanding of the basic biology of tumor-associated vasculature will open the door to new therapeutic targets and the establishment of novel therapies.

In experimental models, tumor-associated VE cells support the maintenance of GSCs[3]. This function can be recapitulated by VE cell-derived conditioned media (CM), suggesting that VE cells produce soluble factors that influence the GSC phenotype. In turn, GSCs can secrete angiogenic factors to promote further neovacularisation[6]. Our recent work has established an interactome network within GBM-associated VE cells and identified key dysregulated genes encoding secreted proteins emanating from VE cells[7]. One such gene is *ESM1* that encodes Endocan, a soluble proteoglycan of 50 kDa, constituted of a mature polypeptide of 165 amino acids (18 kDa) and a single dermatan sulphate chain covalently linked to the serine residue at position 137[8]. *ESM1* expression is regulated by the VEGF/hypoxia pathway and serves as a marker of endothelial cell activation during neoangiogenesis in renal, non-small cell lung, hepatocellular, bladder carcinomas, and GBM[8–10]. *ESM1* is significantly upregulated in tumor-derived vascular cells compared to non-transformed VE cells and its level correlates with higher grade and shorter survival in glioma[11,12]. However, the functional role of Endocan in glioblastoma and, subsequently, its potential as a therapeutic target remains unknown.

In this study using patient-derived GBM and VE cells, syngeneic orthotopic GBM models, and an *Esm1* knockout mouse model[13], we investigated the role of Endocan in intercellular crosstalk between GBM and VE cells. Our findings suggest that targeting Endocan itself or downstream signaling pathways activated by this protein may represent a novel therapeutic approach in the treatment of GBM.

Results

Vascular-secreted Endocan promotes proliferation and migration of GBM cells

To understand how VE cells contribute to the progression of GBM, we tested whether VE cells promote the aggressiveness of GBM *in vitro* and *in vivo* by using two VE cell models: a short-term primary culture of glioblastoma patient-derived VE cells (TEC15) and an immortalized brain VE cell line HBEC-5i. First, we demonstrated that conditioned media (CM) collected from both TEC15 and HBEC-5i cells promote *in vitro* proliferation of gliomasphere lines obtained from four

152 different patients **(Figure 1a** and **Figure S1a)**. Next, we co-injected VE cells (TEC15 or HBEC-
153 5i) with the patient-derived gliomasphere line 1051[14] at a 1:10 ratio into SCID mice, and showed
154 that they significantly shortened animal survival **(Figures 1b, S1b)**. To identify potential trophic
155 factors that could be elaborated by tumor-associated VE cells, we previously isolated $CD31^+$
156 tumor-associated vascular cells from 8 glioblastoma cases along with non-cancerous $CD31^+$
157 cells from 5 craniotomies for epilepsy as controls[7]. Subsequent RNA-sequencing (RNA-seq)
158 revealed *ESM1* as the most significantly upregulated gene in tumor-derived $CD31^+$ cells
159 compared to the non-neoplastic counterparts (**Figure 1c)**. Analysis of a previously published
160 single cell RNAseq database[15] confirmed that *ESM1* is upregulated in one of the endothelial
161 sub-clusters, which was characterized by gene signatures associated with endothelial tip cell
162 formation, tumor angiogenesis, and vascular basement membrane remodeling (**Figures S1c,d**).
163 In the TCGA database, *ESM1* expression was found to correlate with higher glioma grade
164 (**Figure S1e**) and shorter survival of GBM patients (**Figure S1f**). ELISA analysis demonstrated
165 that Endocan, the *ESM1* gene product, was secreted by HBEC-5i and glioblastoma patient-
166 derived VE cells (TEC 14 and TEC15) at concentrations exceeding 100pg/ml, while conditioned
167 media (CM) from normal human astrocytes (NHA) and gliomasphere lines (1079, 157, 711, and
168 1051) contained nearly undetectable amounts of Endocan (**Figure 1d**). We further confirmed
169 this result by immunohistochemical staining (IHC) and demonstrated that Endocan is exclusively
170 co-localized with CD31+ VE cells in the perivascular areas of our GBM clinical samples (**Figure
171 1e**).
172 Next, we investigated whether Endocan could influence GBM phenotype. Incubation with
173 recombinant Endocan (rEndocan) promoted the proliferation of multiple GBM sphere lines
174 **(Figure 1f)**. As GBM cells are known to migrate along blood vessels[16,17], we also examined the
175 effects of Endocan on GBM cell migration using a previously described hydrogel-based
176 system[18]. rEndocan-treated spheroids derived from 3 different patients had significantly
177 enhanced motility as revealed by both migration length (**Figures 1g,h**) and shape factor
178 analysis (**Figure S1g**).
179 Collectively, these findings suggest that vascular-secreted Endocan drive both GBM cell
180 proliferation and migration.
181
182 **Endocan is essential for establishing the hypervascular phenotype of GBM**
183 To address the potential role of paracrine Endocan signaling in crafting the GBM phenotype *in*
184 *vivo*, we utilized wild-type (WT) and *Esm1* knockout (*Esm1* KO) mice[13] as host systems for
185 implanting glioma cells derived from two different murine GBM models. First, we used *in vitro*

186 gliomasphere cultures termed as 7080[19] that was derived from mice harboring mutations in *p53*,
187 *Pten*, and *Nf1* and enriched for the tumor initiating subpopulation[20]. Second, we utilized freshly-
188 resected murine glioblastoma-like cells isolated from tumors induced by RCAS-PDGAB
189 lentivirus injection into Nestin-Tva/Cdkn2a-/- mice[21]. Both types of cancer cells were injected
190 into the brains of WT and *Esm1* KO mice. The resultant tumors in WT mice exhibited numerous
191 intratumoral hemorrhages in sharp contrast to grayish necrotic tumors in *Esm1* KO mice
192 (**Figures 2a, S2a**). Subsequent IHC for CD31 demonstrated significantly fewer $CD31^+$ VE cells
193 in the tumors from *Esm1* KO animals with reduced vessel diameter as compared to those
194 formed in wildtype animals (**Figures 2a-b**, **S2a-b**). At the ultrastructural level, 7080 tumors in
195 the WT host exhibited proliferative blood vessels with hypertrophy and the basement membrane
196 showed an irregular outline and varying diameters, typical of human glioblastoma[16,22], while in
197 the *Esm1* KO host tumors exhibited sparse blood vessels with a regular basement membrane
198 measured as Blood vessel ratio-SAE using previously defined methods[23] (**Figures 2c-d**).
199 Consistent with these observations , qRT-PCR analysis demonstrated that vascular cell-
200 associated genes known to play an integral part in maintaining barrier function, adhesion
201 interactions, and tight junctions(*Podxl*, *Cld5*, and *Cdh5*)[24,25], along with a marker for endothelial
202 cells (*Pecam1*)[15] were downregulated in tumors from *Esm1* KO mice (**Figure S2d**). Importantly,
203 brain vascularization in the areas that did not contain tumor was not appreciably different
204 between wild type and *Esm1* knockout mice, as can be seen from CD31 staining (**Figures s2c**)
205 and electron microscopy (**Figures 2c-d**).
206 We then performed RNA-seq expression profiling of tumors formed by 7080 cells in WT
207 and *Esm1* KO mice and identified 1449 downregulated and 283 upregulated genes (fold change
208 >4; adjusted p-value < 0.05) in KO samples. Subsequent Gene Set Enrichment analysis
209 (GSEA) revealed alterations in many important pathways including downregulation of the
210 proliferation, DNA repair as well as Myc and VEGFA signaling in tumors formed in *Esm1* KO
211 mice (**Figure S2e** and **Table S1)**.
212 Thus far, our findings indicate that Endocan promotes the hypervascularization
213 phenotype of murine gliomas. This effect can be mediated either by autocrine (GBM cells
214 promote Endocan expression in VE cells, which further enhance proliferation of VE cells) or
215 paracrine (GBM cells treated with Endocan secrete other factors which promote vascular cell
216 growth) mechanisms, or a combination of the two. In order to discriminate between these
217 hypotheses, we first treated two human TEC cell lines with rEndocan and in both cases
218 observed a significant increase in proliferation in response to Endocan (**Figure 2e)**. Next, to test
219 the potential for an indirect effect of Endocan on endothelial cells, we treated GBM cells with

220 rEndocan for 3 days, and then replaced the rEndocan containing media with regular GBM
221 media. After 4 more days of incubation, conditioned media was collected and added to TECs.
222 Results of this experiment demonstrated significantly higher proliferation of TECs in Endocan-
223 induced conditioned media compared to the control media (**Figure 2f**).
224 Altogether our data suggest that Endocan is essential for the development of
225 neovascularization in GBM. This protein, secreted by tumor-associated VE cells, can directly
226 enhance proliferation of VE cells within GBM and also can stimulate GBM cells to secrete other
227 factors additionally promoting vascularization of the malignancy.
228
229 **Endocan induces stable phenotypic alterations of GBM cells regulating their spatial**
230 **identity**
231 Next, we aimed to assess if GBM cells propagated *in vivo* in a microenvironment with or without
232 Endocan acquire any stable differences in their phenotype. To answer this question, we
233 generated sphere cultures from tumors formed in WT and *Esm1* KO mice brains (WTD and
234 KOD cells respectively). Even under identical *in vitro* cultivation conditions, KOD GBM cells had
235 reduced proliferation compared to WTD counterparts. Furthermore, KOD cells no longer
236 responded to the addition of rEndocan (**Figure 3a**). To further characterize differences between
237 these cells, we labeled WTD and KOD cells with GFP and mCherry, respectively, and co-
238 injected them into the brains of *Esm1* WT mice (**Figure 3b**). IHC analysis of the resultant tumors
239 demonstrated that WTD cells were located at the tumor edge region and infiltrated into the
240 normal brain, whereas KOD cells appeared to be largely confined to the tumor core (**Figures**
241 **3c, d**). To quantitatively assess this phenomenon, we measured the number of cells of each
242 type as a function of the distance from the injection site, demonstrating that KOD cells were
243 mainly present in the tumor core-region, whereas WTD cells were found to be highly migratory
244 and spread across the tumor and normal brain (**Figure 3e**). Interestingly, CD31 staining
245 indicated that the core lesion predominantly formed by KOD cells was hypovascular, while the
246 edge lesion created mainly by WTD cells was hypervascular (**Figure 3f**). The tumor core areas
247 exhibited higher immunoreactivity to hypoxic and mesenchymal GBM markers (HIF1α, YKL-40,
248 p-65 NF-κB and ALDH1A3)[26–29] (**Figure 3f** and **Figure S3**), while the edge regions had higher
249 levels of proneural markers PDGFRA and Olig2 (**Figure S3**). Taken together, these findings
250 suggest that KOD cells have lost their capacity to promote neovascularization and to invade into
251 the normal tissues even in the presence of Endocan.
252 Surprisingly, we did not observe any survival differences between mice injected with
253 WTD or KOD cells (**Figure 3g**). However, when a mixture of KOD and WTD cells was co-

injected into the brain, animal survival was substantially reduced compared to the mice injected with either KOD or WTD cells alone (**Figure 3g**). We can speculate that the decreased survival of mice injected with the mixture of KOD and WTD cells may be explained by the increased intratumoral heterogeneity which by various mechanisms has been shown to promote GBM malignancy[28,30].

Altogether, the striking differences observed between WTD and KOD cells suggestthat Endocan itself or the tumor microenvironment formed in the presence or absence of Endocan has a significant and long-lasting effect on the key vascular and infiltrative properties of GBM cells. Importantly, the phenotypical differences developed between cells propagated with or without Endocan can be stably maintained even if the cells are subsequently cultured under identical conditions *in vitro* or *in vivo*.

Endocan binds to and activates PDGFRA in human glioblastoma cells

As a next step, we sought to understand the relevant mode of action of Endocan in glioblastoma. To identify possible receptors for Endocan on GBM cells, we purified integral membrane proteins from human gliomasphere line 157 and incubated these proteins with immobilized rEndocan. Subsequent elution of bound proteins and mass spectrometry identified PDGFRA as a potential Endocan-interacting protein (**Table S2**). To confirm this finding in a cell-free system, we tested the binding of the corresponding recombinant proteins. Pull down experiments demonstrated physical interaction between F_c-tagged PDGFRA and His-tagged rEndocan (**Figure 4a)**. As another validation step, we used the proximal ligation assay[31], which showed that rEndocan induces the dimerization of PDGFRA - the initial step in PDGFRA activation[32] (**Figure S4a**). To further confirm the specificity and affinity of Endocan-interaction with PDGFRA, we performed a binding competition assay between rEndocan labeled with Alexa488 and recombinant PDGF-BB (one of the cognate ligands for PDGFRA), labeled with Alexa647. The addition of rPDGF-BB diminished rEndocan binding to glioblastoma cells in a concentration-dependent manner. Similarly, rEndocan decreased rPDGF-BB binding. Importantly, a concentration of 10 ug/ml rEndocan was able to completely displace rPDGFββ from GBM cells, while rPDGF-BB at the corresponding concentration was able to displace only half of the rEndocan molecules (**Figures 4b-c**), suggesting that Endocan can interact with other receptors in addition to PDGFRA.

Given that PDGFRA activation by functional ligands induces receptor autophosphorylation, we investigated whether the addition of rEndocan alters the phosphorylation levels of PDGFRA in human gliomaspheres *in vitro* using PDGF-BB as a

288 positive control[33]. We found that rEndocan (10 ng/ml, 400 pM) was able to induce appreciable
289 autophosphorylation of PDGFRA in as early as 15 minutes and displayed similar temporal
290 kinetics to that of rPDGF-BB (**Figures 4d** and **Figure S4b**). rEndocan treatment also resulted in
291 the phosphorylation of the PDGFRA downstream targets such as p85α and PI3K[34] along with
292 phosphorylation of p44/42 MAPK[35], further confirming the activation of the PDGFRA signaling
293 pathway (**Figures 4d** and **Figure S4b**).
294 Next, we studied how Endocan and PDGF-BB affect GBM cells at the transcriptome
295 level. RNA-seq analysis revealed that their effect on GBM cells was similar but not precisely the
296 same (**Figure 4e**). More than 30% of Endocan-affected genes were not changed by the addition
297 of PDGF-BB, indicating that while Endocan can activate the PDGFRA receptor, it might also
298 have effects that are distinct from those of other PDGFR ligands, possibly due to the binding
299 with other cellular receptors. Gene Set Enrichment Analysis (GSEA) revealed that Endocan
300 specifically affects genes involved in angiogenesis, upregulation of Myc targets, and receptor
301 tyrosine kinase (RTK) pathway activation (**Figure S4c**).
302 Finally, we evaluated the feasibility of Endocan and PDGFRA interactions in brain
303 tumors using IHC. The staining of patient tumors demonstrated the presence of Endocan-
304 expressing cells within perivascular areas that are adjacent to PDGFRA^{+} cells (**Figure 4f**).
305 Altogether, our data indicate that one of the molecular mechanisms by which Endocan
306 affects GBM is binding to PDGFRA and subsequent activation of the downstream signaling
307 pathways in tumor cells adjacent to VE cells in the microvasculature proliferation area.
308
309 **Endocan induces changes in the chromatin structure in the *Myc* promoter region**
310 Since we demonstrated that GBM cells propagated in *Esm1* KO and WT mice showed
311 substantial and highly persistent phenotypic differences, we hypothesized that Endocan-
312 PDGFRA signaling can induce stable epigenetic alterations. To test this hypothesis, we
313 performed ATAC-seq (Assay for Transposase-Accessible Chromatin sequencing) with *Esm1*
314 WTD and KOD cells[36]. We identified 38 genes that had significantly different chromatin
315 accessibility levels between samples, and among them, 9 genes showed different chromatin
316 structure in their promoter regions (**Figures 5a and Table S3**). The strongest alterations were
317 observed for the *Myc* promoter that showed more than 10-fold increased accessibility in WTD
318 as opposed to KOD cells. To explore the relationship between open chromatin structure and
319 gene expression levels, we next performed RNA-seq analysis of the same samples (**Figures**
320 **5b-c and Table S4**). Comparison of ATAC-seq and RNA-seq data revealed that among all
321 genes with altered chromatin structure, *Myc* had the most substantial upregulation in the

322 expression, with WTD tumors showing 25-folds higher level of *Myc* mRNA than KOD samples. ,
323 IHC of WTD tumors revealed higher expression of c-Myc as compared to *Esm1* KOD samples
324 (**Figure 5d**). To further confirm these data, we performed WB analysis for PDGFRA and Myc in
325 the corresponding cells and saw consistent loss in the expression of both of these proteins in
326 *Esm1* KOD samples (**Figure 5e**). To validate our finding that Myc is a downstream target of
327 Endocan-driven PDGFRA signaling, we first treated our WTD and KOD cells with 10ng/ml of
328 rEndocan for 3 days and found robust upregulation of *Myc* expression in WTD cells but not in
329 *Esm*1 KOD cells (**Figure 5f**). Next, we used *in vitro* culture of patient-derived GBM cells (1079,
330 408 and 413) and confirmed that Myc was significantly upregulated at both the mRNA and
331 protein levels in response to addition of the rEndocan to all tested cells (**Figures 5g-i, S5**).
332
333 **Inhibition of the PDGFRA pathway attenuates the effect of Endocan on GBM cells**
334 We next investigated whether the inhibition PDGFRA signaling would affect Myc
335 expression. First, using lentiviral knockdown, we demonstrated that Myc level was substantially
336 reduced upon depletion of PDGFRA (**Figure 6a**). Knockdown of PDGFRA also abrogated the
337 proproliferative effect of Endocan on GBM cells (**Figure 6b**). Second, we utilized small molecule
338 inhibitors ponatinib[37] and nintedanib[38] that have a high relative selectivity toward PDGFRA. Our
339 results demonstrated that both compounds abrogate the effect of Endocan on PDGFRA
340 activation and diminish Myc expression (**Figures 6c** and **Figure S6a, b**). , Treatment of GBM
341 cells with ponatinib also reduced the proproliferative effect of rEndocan (**Figure 6d**).
342 Based on these data, we hypothesized that blockade of PDGFRA signaling in the WT
343 background would attenuate Endocan-mediated activation of PDGFRA and subsequent Myc
344 upregulation, leading to a hypovascular phenotype similar to that observed in *Esm1* KO tumors
345 (**Figure 2**). To this end, we treated WT and *Esm1* KO mice bearing 7080 tumor cells with
346 ponatinib. Consistent with our hypothesis, ponatinib enhanced survival only of the tumor-bearing
347 WT, but not *Esm1* KO mice (**Figure 6e**), and reduced blood vessel formation, as can be seen
348 from both CD31 immunostaining intensity (**Figure 6f**) and quantification of the blood vessels
349 diameter (**Figure 6g).** Furthermore, IHC staining demonstrated that treatment with ponatinib
350 resulted in a loss of Myc and Olig2 expression accompanied by increased level of p65-NFkB, a
351 marker associated with tumor core (hypovascular) cells[26] **(Figure S6c)**. Importantly, this effect
352 was only observed in *Esm1* WT bot not KO mice.
353 Taken together, our findings suggest that Endocan-induced PDGFRA activation affects
354 chromatin structure of the Myc promoter region leading to the prolonged upregulation of Myc
355 expression and stable phenotypic alterations of GBM cells. Importantly, this pathway can be

356 inhibited by small molecule compounds targeting PDGFRA. Tumors formed in the absence of
357 Endocan utilize other mechanisms to drive their growth and are less sensitive to PDGFRA
358 inhibitors.
359
360 **Endocan protects glioblastoma cells from radiotherapy**
361 Previous studies have demonstrated that the tumor vascular niche provides protection to GBM
362 cells against radiotherapy (IR)[39]. Therefore, we sought to determine the role of Endocan
363 signaling in this process. First, we demonstrated that IR substantially upregulated *ESM1*
364 transcription in VE cells *in vitro* as measured by qRT-PCR (**Figure S7a)** and increased
365 secretion of Endocan protein by more than 3 folds as determined by ELISA (**Figure 7a**). Given
366 these findings, we assessed whether IR-induced upregulation of Endocan could play a role in
367 radioprotection of GBM cells by VE cells. First, we pretreated GBM cells with rEndocan or
368 HBEC-5i conditioned medium (CM) for 3 days, followed by IR at 8 Gy. Analysis of
369 gliomaspheres on day 5 post-irradiation revealed that both rEndocan and HBEC-5i CM
370 significantly decreased IR-induced apoptosis (**Figure 7b** and **Figure S7b)**, prevented cell-cycle
371 arrest (**Figure S7c**), and promoted GBM cell survival after radiation treatment (**Figures S7d)**.
372 Furthermore, cells pretreated with Endocan had significantly reduced γ-H2AX staining intensity
373 compared to the control groups (**Figure 7c**), indicating diminished IR-induced DNA damage[40].
374 Finally, given that radiation promotes mesenchymal differentiation of gliomaspheres[26], we
375 examined the effect of Endocan on the expression levels of mesenchymal (CD44) and
376 proneuronal (CD133) GBM markers in irradiated 1051 cells. Pretreatment with either HBEC-5i
377 CM or rEndocan suppressed radiation-induced downregulation of CD133 and upregulation of
378 CD44 (**Figure S7e**), and therefore, protected GBM cells from mesenchymal differentiation.
379 To confirm that the protective effect of the secretomes from VE cells was specifically
380 mediated by Endocan protein but not by other factors, we depleted Endocan from HBEC-5i CM
381 using an anti-Endocan antibody. This depletion resulted in a decrease in the radioprotection of
382 the HBEC-5i CM as measured by caspase 3/7 activity assay and a cellular proliferation assay
383 (**Figure 7d**, **S7f**). RNA-seq of gliomaspheres that were pretreated with either HBEC-5i CM or
384 rEndocan and subsequently exposed to 8 Gy IR demonstrated that rEndocan largely
385 recapitulated the effects of HBEC-5i CM on the transcriptome of gliomaspheres after irradiation
386 (**Figure 7e**). These findings suggest that Endocan is the major mediator for the VE cell-driven
387 radioprotective effect on glioblastoma cells.
388 Finally, we investigated the effect of radiation treatment on survival of tumor-bearing
389 *Esm1* WT and KO mice (**Figure 7f**). Both tumor models showed substantial shrinkage in size

390 after radiation. However, radiation treatment resulted in a significantly greater enhancement of
391 survival of tumor-bearing KO mice than WT mice (**Figure 7f, S7g**). These results are in a good
392 agreement with our RNAseq data that demonstrated downregulation of DNA repair pathway in
393 tumors formed in *Esm1* KO animal (**Figure S2e)**.
394 Altogether, our findings demonstrate that Endocan is a key mediator of the
395 radioprotective effect of VE cells on GBM cells. Importantly, Endocan secretion is additionally
396 increased upon IR which further promotes GBM cell viability and prevents radiation-induced
397 mesenchymal differentiation of glioblastoma cells.
398
399 **Discussion**
400 More than 50 years ago, it was demonstrated that malignant tumors promote microvascular
401 proliferation, which in turn provides nutritional support that enables further cancer progression[41].
402 However, during the last decade, it has become clear that the relationship between tumor and
403 VE cells is far more complicated. They form a sophisticated multilayered interaction network that
404 shapes the key properties of both cell types. Although many components of this crosstalk have
405 been identified, the key factors that orchestrate the entirety of tumor-vasculature signaling are
406 not well elucidated. In the current study, we investigated some of the mechanisms of
407 bidirectional interactions between GBM and VE cells. A dataset generated during our previous
408 work allowed us to identify Endocan (*ESM1* gene) as the most significantly upregulated
409 secreted protein in tumor-associated VE cells when compared to the normal brain endothelium.
410 Our experiments revealed that on the one hand, Endocan affects the phenotype of GBM cells,
411 and on the other hand, by direct and indirect mechanisms further promotes microvascular
412 proliferation within the tumor (**Figure. 8**). Using *Esm1* KO mice, we demonstrated that the
413 absence of Endocan has a dramatic effect on both GBM cells and tumor-associated
414 vasculature, suggesting that this protein might be one of the master regulators of GBM-VE
415 crosstalk.
416 A previous study demonstrated that Endocan and vascular endothelial growth factor A
417 (VEGF-A) form a positive feedback loop in which VEGF-A promotes expression of Endocan in
418 endothelial tip cells while Endocan further increases bioavailability of VEGF-A[13]. Considering
419 that VEGF-A is one of the key vasculature growth factors secreted by cancer cells, Endocan
420 upregulation in GBM-associated VE cells is not surprising. Interestingly, prior studies have also
421 implicated Endocan in modulating cell proliferation, migration, and invasion in renal, colorectal,
422 non-small cell lung, and hepatocellular cancers[10], and showed that its expression correlated
423 with poor prognosis in GBM patients[7]. Our data provide mechanistic explanations of these

424 findings and suggest Endocan as a possible target for therapy as well as a potential diagnostic
425 marker that may be used to predict GBM sensitivity to various types of treatment.
426 To determine the molecular mechanism by which Endocan affects GBM, we first
427 identified its receptor on the surface of GBM cells. We demonstrated that Endocan binds to and
428 activates PDGFRA which subsequently phosphorylates multiple downstream targets such as
429 PI3K and ERK[42]. Endocan was previously shown to interact with CD11a integrin in human
430 lymphocytes and Jurkat cells[43] and that it could also activate EGFR signaling in non-small cell
431 lung cancer[44]. However, our analysis did not identify either EGFR or CD11a as Endocan binding
432 partners in GBM. It is possible that due to its unique structure that contains N-terminal 18 kDa
433 protein component and C-terminal 30 kDa dermatan sulfate chain Endocan can interact with a
434 high variety of cell surface receptors as well as extracellular matrix components[13], and the net
435 functional outcome of Endocan will depend on the expression level of its binding partners in
436 addition to its relative affinity for them. This hypothesis is in good agreement with our data
437 indicating that Endocan has a similar but not identical effect as PDGF-BB– one of the cognate
438 ligands of PDGFRA, suggesting that Endocan may activate other yet unknown receptors in
439 GBM. However, as we demonstrated that PDGFRA inhibition is sufficient to abrogate the effect
440 of Endocan on GBM cells, we can speculate that, at least in our experimental model, PDGFRA
441 is the main receptor for Endocan. Importantly, these data also provide insights into the non-
442 canonical mechanisms of PDGFRA activation. Although the classical ligands for PDGFRs are
443 members of PDGF family, other ligands for these receptors such as VEGF-A[45] and CTGF[46]
444 have been identified. Therefore, Endocan may serve an additional PDGFR ligand allowing
445 cancer cells to activate PDGFRA signaling pathway, even if PDGFs are absent or diminished
446 Somewhat surprisingly, our results demonstrated that Endocan itself or
447 microenvironmental conditions formed *in vivo* in the presence or absence of Endocan induce
448 highly stable phenotypic alterations of GBM cells that persist even after months of cultivation in
449 identical conditions. As this result was reproduced in two substantially different mouse GBM
450 models, we hypothesized that it was associated with epigenetic alterations rather than with *de*
451 *novo* mutations arising during propagation. Subsequent experiments revealed that while,
452 overall, chromatin structure of GBM cells propagated in ESM1 WT and KO mice was very
453 similar, there was a substantial difference in Myc promoter accessibilitydifference in the
454 chromatin accessibility in the *Myc* gene.. Consistent with these findings, we demonstrated
455 upregulation of Myc at both protein and mRNA levels. These results are in good agreement with
456 previously published data indicating that PDGFR activation promotes Myc expression[47] and that
457 Myc level is regulated by the chromatin structure of its promoter region[48]. However, the exact

molecular mechanism whereby PDGFR activation leads to altered chromatin and elevated Myc expression remains unknown.

As most of our experiments demonstrated that Endocan promotes aggressiveness of GBM cells, one could expect that GBM tumors developed in the presence of Endocan would show more malignant properties than the Endocan-deprived counterpart. Surprisingly, this was not the case. We demonstrated that GBM cells propagated in *Esm1* KO mice were as aggressive as the ones in *Esm1* WT. Nevertheless, our further experiments revealed that Endocan does increase the malignancy of GBM if cancer cells propagated in ESM1 WT and KO mice are co-injected together into the same animal. These findings are in good agreement with previous work indicating that a higher level of GBM intratumoral heterogeneity, rather than any specific tumor phenotype, correlates with worse patient outcome[49]. We can speculate that Endocan secretion restricted to the perivascular niche enhances intratumoral heterogeneity by promoting the development of two phenotypically distinct cell populations that grow in the presence or absence of Endocan. In our previous studies, we demonstrated that a variety of factors in the tumor necrotic core microenvironment promote mesenchymal-like transformation of GBM cells[28,50]. It is interesting to propose that the opposite process may exist in regions of microvascular proliferation, where Endocan protects GBM cells from mesenchymal differentiation and stimulates more proneural-like properties. This hypothesis is indirectly confirmed by the observation that Myc signaling is upregulated in proneural GBM tumors, while the mesenchymal ones exploit pathways related to inflammatory response and IL6/JAK/STAT3[51]. Therefore, we can argue that in different GBM regions various microenvironmental factors may differentially affect GBM phenotype, thereby promoting intratumoral heterogeneity and increasing GBM malignancy, and that Endocan protein plays an important role in this process.

We found that Endocan had a broad effect on GBM cell phenotype: it i) promoted cell migration; ii) enhanced proliferation; iii) increased resistance to therapy; iv) protected GBM cells from radiation induced mesenchymal differentiation; and v) stimulated neovascularization. Such multifunctionality can be explained by two scenarios. First, Endocan might interact with different receptors on GBM cells, activating various signaling pathways to produce the broad spectrum of observed effects. A second possibility is that Endocan affects a master regulator of GBM phenotype which is solely responsible for the observed downstream events. Discriminating between these possibilities will be important for the development of Endocan-targeted therapy, as in the first case it will be rational to inhibit Endocan protein itself, while in the second scenario, blocking of Endocan's receptor or its downstream targets might be more beneficial.

While our current data do not allow us to definitively distinguish between these two mechanisms, the majority of our results suggest that most if not all effects of Endocan can be explained by the activation of the PDGFRA-Myc signaling axis. Indeed, Myc is known to act as a master regulator of angiogenic factors in GBM and other solid tumors[55] and is also heavily involved in the regulation of GBM stemness, radioresistance and metabolisms[52,53]. However, further studies are needed to precisely dissect the molecular mechanisms underlying the effect of Endocan on GBM cells.

From the therapeutic perspective, blockade of Endocan signaling in GBM cells can be achieved by at least four different approaches: i) downregulation of Endocan secretion in VE cells; ii) removal of the already secreted Endocan protein from the extracellular space; iii) direct inhibition of PDGFRA; and iv) inhibition of Myc. Importantly, we demonstrated that treatment with a PDGFRA inhibitor, ponatinib, more substantially increased survival of animals from the *Esm1* wild-type group as opposed to the *Esm1*-KO mice, indicating that tumors that have a high level of expression of Endocan may be more sensitive to this type of treatment. On the other hand, we showed that the removal of Endocan from conditioned medium by antibodies increases the efficacy of radiotherapy *in vitro*. Consistent with these latter findings, a prior study demonstrated that treatment of mice with metastatic breast cancer tumors with 1-2B7, a high affinity anti-Esm1 monoclonal antibody, yielded an improved response to bevacizumab treatment i*n vivo*[54]. In an alternate approach, the addition of sunitinib (multi-tyrosine kinase inhibitor) to HUVEC endothelial cells has been recently shown to specifically prevent upregulation of Endocan, demonstrating another means to inhibit Endocan-tumor interactions. Finally, although no clinically successful small molecule Myc inhibitors have been developed thus far[55] multiple approaches such as blocking peptides[56] and exosome mediate knockdown[57] have shown promising results in *in vivo* GBM models. It is important to note that global loss of *Esm1* does not cause a noticeable defect in the brain or other organs, so systematically diminishing or even eliminating tumor-associated Endocan could indeed be a promising strategy to control glioblastoma progression and recurrence.

Unfortunately, development of resistance to Endocan-targeting therapy can be expected. Thus, we demonstrated that in the absence of Endocan, GBM cells undergo reprogramming that can desensitize them to PDGFRA inhibition. This coincides well with a recently published study that showed that upon blockade of the PDGFR signaling pathway, GBM cells acquire stable and persistent phenotypic alterations allowing them to rely on PDGF-independent proliferation mechanisms[58]. Therefore, it is important to develop approaches targeting both Endocan-PDGFRA dependent and independent populations of GBM cells within the tumor.

In summary, the findings presented here provide insights into the mechanisms of intercellular crosstalk between GBM and VE. We found that the endothelial secreted Endocan protein has a strong effect on both VE and GBM cells and seems to play an important role in GBM progression. However, similar to the results earlier obtained in a clinical trial of the anti-angiogenic drug bevacizumab which failed to improve overall survival of GBM patients due to metabolic reprograming[59], glioblastoma cells can easily adapt to the absence of Endocan by using alternative signaling pathways. Therefore, in order to achieve progress in the therapy of this devastating disease, it will be critical to reveal the molecular mechanisms underlying the high plasticity and adaptation capacity of GBM cells. Our results point to the alteration in chromatin structure of Myc as one of pathways possibly responsible for such adaptation.

References:

1. Calabrese, C. *et al.* A perivascular niche for brain tumor stem cells. *Cancer cell* **11**, 69–82 (2007).
2. Charles, N. *et al.* Perivascular nitric oxide activates notch signaling and promotes stem-like character in PDGF-induced glioma cells. *Cell stem cell* **6**, 141–152 (2010).
3. Burgett, M. E. *et al.* Direct contact with perivascular tumor cells enhances integrin αvβ3 signaling and migration of endothelial cells. *Oncotarget* **7**, 43852–43867 (2016).
4. Hambardzumyan, D. & Bergers, G. Glioblastoma: Defining Tumor Niches. *Trends Cancer* **1**, 252–265 (2015).
5. Shiraki, Y. *et al.* Significance of perivascular tumour cells defined by CD109 expression in progression of glioma. *The Journal of pathology* **243**, 468–480 (2017).
6. Brooks, L. J. & Parrinello, S. Vascular regulation of glioma stem-like cells: a balancing act. *Current Opinion in Neurobiology* **47**, 8–15 (2017).
7. Ghochani, Y. *et al.* A molecular interactome of the glioblastoma perivascular niche reveals integrin binding sialoprotein as a mediator of tumor cell migration. *Cell Rep* **41**, 111511 (2022).
8. Scherpereel, A. *et al.* Overexpression of endocan induces tumor formation. *Cancer Res* **63**, 6084–6089 (2003).
9. Cai, L. *et al.* Dopamine agonist resistance-related endocan promotes angiogenesis and cells viability of prolactinomas. *Endocrine* **52**, 641–651 (2016).
10. Delehedde, M., Devenyns, L., Maurage, C.-A. & Vivès, R. R. Endocan in cancers: a lesson from a circulating dermatan sulfate proteoglycan. *International journal of cell biology* **2013**, 705027 (2013).
11. Maurage, C.-A. *et al.* Endocan expression and localization in human glioblastomas. *J Neuropathol Exp Neurol* **68**, 633–641 (2009).
12. Zhang, G. *et al.* Chromatin remodeler HELLS maintains glioma stem cells through E2F3 and MYC. *JCI Insight* **4**, e126140, 126140 (2019).
13. Rocha, S. F. *et al.* Esm1 modulates endothelial tip cell behavior and vascular permeability by enhancing VEGF bioavailability. *Circ Res* **115**, 581–590 (2014).
14. Bastola, S. *et al.* Glioma-initiating cells at tumor edge gain signals from tumor core cells to promote their malignancy. *Nat Commun* **11**, 4660 (2020).
15. Xie, Y. *et al.* Key molecular alterations in endothelial cells in human glioblastoma uncovered through single-cell RNA sequencing. *JCI Insight* **6**, e150861 (2021).

16. Cribaro, G. P. *et al.* Three-dimensional vascular microenvironment landscape in human glioblastoma. *Acta Neuropathologica Communications* **9**, 24 (2021).
17. Griveau, A. *et al.* A Glial Signature and Wnt7 Signaling Regulate Glioma-Vascular Interactions and Tumor Microenvironment. *Cancer Cell* **33**, 874-889.e7 (2018).
18. Liang, J. *et al.* Hydrogel Arrays Enable Increased Throughput for Screening Effects of Matrix Components and Therapeutics in 3D Tumor Models. *J Vis Exp* 10.3791/63791 (2022) doi:10.3791/63791.
19. Zhu, Y. *et al.* Early inactivation of p53 tumor suppressor gene cooperating with NF1 loss induces malignant astrocytoma. *Cancer Cell* **8**, 119–130 (2005).
20. Hemmati, H. D. *et al.* Cancerous stem cells can arise from pediatric brain tumors. *Proc Natl Acad Sci U S A* **100**, 15178–15183 (2003).
21. Herting, C. J. *et al.* Tumour-associated macrophage-derived interleukin-1 mediates glioblastoma-associated cerebral oedema. *Brain* **142**, 3834–3851 (2019).
22. Nyström, S. H. M. Electron Microscopical Structure of the Wall of Small Blood Vessels in Human Multiform Glioblastoma. *Nature* **184**, 65–65 (1959).
23. Bartmeyer, P. M., Biscola, N. P. & Havton, L. A. A shape-adjusted ellipse approach corrects for varied axonal dispersion angles and myelination in primate nerve roots. *Sci Rep* **11**, 3150 (2021).
24. Cait, J. *et al.* Podocalyxin is required for maintaining blood–brain barrier function during acute inflammation. *Proceedings of the National Academy of Sciences* **116**, 4518–4527 (2019).
25. Ishihara, H. *et al.* Endothelial Cell Barrier Impairment Induced by Glioblastomas and Transforming Growth Factor β2 Involves Matrix Metalloproteinases and Tight Junction Proteins. *Journal of Neuropathology & Experimental Neurology* **67**, 435–448 (2008).
26. Bhat, K. P. L. *et al.* Mesenchymal differentiation mediated by NF-κB promotes radiation resistance in glioblastoma. *Cancer Cell* **24**, 331–346 (2013).
27. Minata, M. *et al.* Phenotypic Plasticity of Invasive Edge Glioma Stem-like Cells in Response to Ionizing Radiation. *Cell reports* **26**, 1893-1905.e7 (2019).
28. Pavlyukov, M. S. *et al.* Apoptotic Cell-Derived Extracellular Vesicles Promote Malignancy of Glioblastoma Via Intercellular Transfer of Splicing Factors. *Cancer Cell* **34**, 119-135.e10 (2018).
29. Mao, P. *et al.* Mesenchymal glioma stem cells are maintained by activated glycolytic metabolism involving aldehyde dehydrogenase 1A3. *Proc Natl Acad Sci U S A* **110**, 8644–8649 (2013).

30. Neftel, C. *et al.* An Integrative Model of Cellular States, Plasticity, and Genetics for Glioblastoma. *Cell* **178**, 835-849.e21 (2019).
31. Alam, M. S. Proximity Ligation Assay (PLA). *Curr Protoc Immunol* **123**, e58 (2018).
32. Martinho, O. *et al.* Expression, mutation and copy number analysis of platelet-derived growth factor receptor A (PDGFRA) and its ligand PDGFA in gliomas. *Br J Cancer* **101**, 973–982 (2009).
33. Raica, M. & Cimpean, A. M. Platelet-Derived Growth Factor (PDGF)/PDGF Receptors (PDGFR) Axis as Target for Antitumor and Antiangiogenic Therapy. *Pharmaceuticals (Basel)* **3**, 572–599 (2010).
34. MacDonald, T. J. *et al.* Expression profiling of medulloblastoma: PDGFRA and the RAS/MAPK pathway as therapeutic targets for metastatic disease. *Nat Genet* **29**, 143–152 (2001).
35. Conway, A. M., Rakhit, S., Pyne, S. & Pyne, N. J. Platelet-derived-growth-factor stimulation of the p42/p44 mitogen-activated protein kinase pathway in airway smooth muscle: role of pertussis-toxin-sensitive G-proteins, c-Src tyrosine kinases and phosphoinositide 3-kinase. *Biochem J* **337 (Pt 2)**, 171–177 (1999).
36. Buenrostro, J. D., Wu, B., Chang, H. Y. & Greenleaf, W. J. ATAC-seq: A Method for Assaying Chromatin Accessibility Genome-Wide. *Curr Protoc Mol Biol* **109**, 21.29.1-21.29.9 (2015).
37. Lee, E. Q. *et al.* Phase II trial of ponatinib in patients with bevacizumab-refractory glioblastoma. *Cancer Med* **8**, 5988–5994 (2019).
38. Phase II open-label study of nintedanib in patients with recurrent glioblastoma multiforme - PubMed. https://pubmed.ncbi.nlm.nih.gov/23184145/.
39. Muthukrishnan, S. D. *et al.* P300 promotes tumor recurrence by regulating radiation-induced conversion of glioma stem cells to vascular-like cells. *Nat Commun* **13**, 6202 (2022).
40. Kuo, L. J. & Yang, L.-X. Gamma-H2AX - a novel biomarker for DNA double-strand breaks. *In Vivo* **22**, 305–309 (2008).
41. Folkman, J. Tumor angiogenesis: therapeutic implications. *N Engl J Med* **285**, 1182–1186 (1971).
42. Werth, C. *et al.* Stromal resistance of fibroblasts against oxidative damage: involvement of tumor cell-secreted platelet-derived growth factor (PDGF) and phosphoinositide 3-kinase (PI3K) activation. *Carcinogenesis* **29**, 404–410 (2008).

43. Béchard, D. *et al.* Human endothelial-cell specific molecule-1 binds directly to the integrin CD11a/CD18 (LFA-1) and blocks binding to intercellular adhesion molecule-1. *J Immunol* **167**, 3099–3106 (2001).
44. Yang, Y.-C. *et al.* Circulating Proteoglycan Endocan Mediates EGFR-Driven Progression of Non-Small Cell Lung Cancer. *Cancer research* **80**, 3292–3304 (2020).
45. Ball, S. G., Shuttleworth, C. A. & Kielty, C. M. Vascular endothelial growth factor can signal through platelet-derived growth factor receptors. *J Cell Biol* **177**, 489–500 (2007).
46. Pi, L. *et al.* Connective tissue growth factor differentially binds to members of the cystine knot superfamily and potentiates platelet-derived growth factor-B signaling in rabbit corneal fibroblast cells. *World Journal of Biological Chemistry* **6**, 379–388 (2015).
47. Frontiers | SHP-2-Induced Activation of c-Myc Is Involved in PDGF-B-Regulated Cell Proliferation and Angiogenesis in RMECs. https://www.frontiersin.org/articles/10.3389/fphys.2020.555006/full.
48. Rahmat, M. *et al.* Identification of a Novel Epigenetic Mechanism of MYC Deregulation in Smoldering and Newly Diagnosed Multiple Myeloma Patients. *Blood* **138**, 504 (2021).
49. Patel, A. P. *et al.* Single-cell RNA-seq highlights intratumoral heterogeneity in primary glioblastoma. *Science* **344**, 1396–1401 (2014).
50. Larionova, T. D. *et al.* Alternative RNA splicing modulates ribosomal composition and determines the spatial phenotype of glioblastoma cells. *Nat Cell Biol* **24**, 1541–1557 (2022).
51. Kersch, C. N. *et al.* Transcriptional signatures in histologic structures within glioblastoma tumors may predict personalized drug sensitivity and survival. *Neuro-Oncology Advances* **2**, vdaa093 (2020).
52. IJMS | Free Full-Text | The “Superoncogene” Myc at the Crossroad between Metabolism and Gene Expression in Glioblastoma Multiforme. https://www.mdpi.com/1422-0067/24/4/4217.
53. Zhou, L. *et al.* PSMG3-AS1 enhances glioma resistance to temozolomide via stabilizing c-Myc in the nucleus. *Brain and Behavior* **12**, e2531 (2022).
54. Kang, N. *et al.* Endothelial-Specific Molecule 1 Inhibition Lessens Productive Angiogenesis and Tumor Metastasis to Overcome Bevacizumab Resistance. *Cancers* **14**, 5681 (2022).
55. Llombart, V. & Mansour, M. R. Therapeutic targeting of ‘undruggable’ MYC. *EBioMedicine* **75**, 103756 (2022).
56. Dhungel, L., Harris, C., Romine, L., Sarkaria, J. & Raucher, D. Targeted c-Myc Inhibition and Systemic Temozolomide Therapy Extend Survival in Glioblastoma Xenografts. *Bioengineering* **10**, 718 (2023).

57. Haltom, A. R. *et al.* Engineered exosomes targeting MYC reverse the proneural-mesenchymal transition and extend survival of glioblastoma. *Extracell Vesicle* **1**, 100014 (2022).
58. Lam, K. H. B. *et al.* Topographic mapping of the glioblastoma proteome reveals a triple-axis model of intra-tumoral heterogeneity. *Nat Commun* **13**, 116 (2022).
59. Fack, F. *et al.* Bevacizumab treatment induces metabolic adaptation toward anaerobic metabolism in glioblastomas. *Acta Neuropathol* **129**, 115–131 (2015).
60. Gotlib, L. J. & Searls, D. B. Plasma membrane isolation on DEAE-Sephadex beads. *Biochim Biophys Acta* **602**, 207–212 (1980).
61. IHC Profiler: An Open Source Plugin for the Quantitative Evaluation and Automated Scoring of Immunohistochemistry Images of Human Tissue Samples | PLOS ONE. https://journals.plos.org/plosone/article?id=10.1371/journal.pone.0096801.

726 **Materials and Methods**

727 **Informed consent and ethics committee approvals:** This study was conducted under
728 protocols approved by the IRBs and IACUCs of University of California Los Angeles (UCLA),
729 MD Anderson Cancer Center (MDA), and University of Alabama at Birmingham (UAB).

730 **Cell cultures**: Human gliomasphere cultures were maintained in DMEM/F12 medium
731 supplemented with 2% B27 supplement (% vol), 20 ng/ml bFGF, and 20 ng/ml EGF. The bFGF
732 and EGF were added twice a week, and the culture medium was replaced every 7 days.
733 Experiments with neurospheres/gliomaspheres were performed with lines that were cultured for
734 fewer than 30 passages since their initial establishment. To obtain Human Tumor-Associated
735 Endothelial cell culture glioblastoma tissues from patients were freshly isolated during surgery,
736 manually dissociated into single cells, and subsequently sorted for CD31+ cells using magnetic
737 beads (ThermoFisher Scientific). Following confirmation of CD31 expression, VE cells were
738 grown in fibronectin-coated flasks with Endothelial cell growth media (ScienCell) containing 2%
739 FBS, 1% Penicillin-Streptomycin solution and 1% Endothelial growth supplement (ScienCell).
740 HBEC-5i (ATCC) were cultivated in DMEM/F12 medium containing 10% FBS, 1% Penicillin-
741 Streptomycin solution and 1% Endothelial cell growth supplement. Expression of CD31 was
742 periodically checked by flow cytometry. Spontaneous tumors formed in *PTEN*, *TP53*, *NF1*
743 deleted mice[19] were grown in neurosphere media as described previously. Freshly obtained
744 mice tumor (PDGFB-overexpressing mouse GBM model) was kindly shared by Dolores
745 Hambardzyuman lab (Emory University). Tumors were isolated to obtain single cells for injection
746 into mice. HBEC-5i (ATCC) cells were cultivated in DMEM/F12 medium containing 10% FBS,
747 1% Penicillin-Streptomycin solution and 1% Endothelial cell growth supplement. STR analysis
748 was performed to confirm cell identity (**Table S5**). The cell lines were tested negative for
749 mycoplasma contamination.

750 **Genetically modified mice:** *Esm1* KO (Bl/6) mice are a generous gift from Dr. Ralf H. Adams[13].
751 All animals were maintained in accordance with the National Institute of Health (NIH) Guide for
752 the care and Use of Laboratory Animals and were handled according to protocols approved by
753 the University of Alabama at Birmingham Institutional Animal Care and Use Committee. The
754 genomic status of *Esm1* was confirmed by PCR according to the prior studies.

755 ***In Vivo* Intracranial Xenograft Tumor Models**: 6-8-week-old NOD SCID mice (Prkdc^{scid}) were
756 used for intracranial tumor formation. In each mouse, 5 x 10^5 cells of human patient-derived
757 glioblastoma cells were injected Detailed protocol is described previously[7,14].

758 ***In Vivo* Syngeneic Intracranial Tumor Models:** Our general protocol for the intracranial tumor
759 models was described previously[14]. Briefly, 5 x 10^5 murine glioblastoma cells were injected into
760 the brains of Bl/6 or *Esm1* KO mice. Mice were monitored and sacrificed when
761 neuropathological symptoms developed. For immunohistochemical studies, mice were perfused
762 with ice-cold PBS, followed by 4% paraformaldehyde (PFA). Mice brains were dissected and
763 fixed in 4 % PFA solution for 48 hours and then transferred to 10% formalin for 48 hours. For
764 tumor collection to perform RNA extraction, mice were sacrificed, and tumors were isolated and
765 fast-frozen using liquid nitrogen.

766 ***In vitro* and *in vivo* irradiation**: Cells or mice were irradiated at room temperature using X-ray
767 irradiator (Gulmay Medical Inc., Atlanta, GA) at a dose rate of 5.519 Gy/min for the time
768 required to apply an 8Gy dose. The X-ray beam was calibrated using NIST-traceable dosimetry
769 and operated at 300kV and hardened using a 4mm Be, a 3mm Al, and a 1.5mm Cu filter. Mice
770 were anesthetized prior to the irradiation. The body was covered with lead shield to avoid whole
771 body irradiation.

772 ***In vivo* drug treatments:** Mice were injected with 7080 cells to form intracranial tumors. On day
773 14 post injection, mice were given daily administration of 50mg/kg/day of Ponatinib
774 (Selleckchem) by oral gavage for 5 days.

775 **Endocan enzyme-linked immunosorbent assay (ELISA):** The concentration of secreted
776 Endocan was measured in conditioned medium using the Endocan ELISA kit (Boster Bio)
777 according to the manufacturer's protocol.

778 **Protein labeling:** Recombinant Endocan and PDGF-BB were labeled with Alexa Fluor 488
779 Microscale Protein Labeling Kit (Thermo Fisher Scientific) and Alexa Fluor™ 647 Microscale
780 Protein Labeling Kit (Thermo Fisher Scientific) respectively according to the manufacturer's
781 protocol. Labeled proteins were added to glioblastoma cells in different concentrations and after
782 30 min incubation on ice, cells were washed twice with PBS and analyzed by Attune NxT Flow
783 Cytometer (Thermo Fisher Scientific). The obtained data were processed with FlowJo 10
784 software.

785 **Recombinant protein pull-down assay:** To obtain a protein complex, recombinant His-tagged
786 Endocan (R&D) was immobilized on 50 µl of HisPur Ni-NTA Magnetic Beads (Thermo Fisher
787 Scientific) according to the manufacturer's protocol. The beads were washed 3 times with PBS

788 and incubated for 2 hours with Fc-tagged recombinant PDGFRA (R&D) under constant
789 agitation. Next, beads were washed 3 times with PBS and bounded proteins were eluted with
790 300 mM imidazole in PBS and subjected to subsequent western blot analysis.
791
792 **Proximal Ligation Assay:** Glioblastoma cells were plated in wells of Lab-Tek II chamber pre-
793 coated with laminin and treated with Endocan or PDGFBB for 90 minutes. Next, cells were
794 washed 3 times with phosphate-buffered saline (PBS) and fixed with 4% PFA in PBS for 15 min
795 at room temperature. Cells were washed 2 times with PBS and permeabilized with 0.2% Triton-
796 X100 in PBS for 15 minutes. All subsequent procedures were performed using "Duolink In Situ
797 Orange Starter Kit" (Duolink) according to the manufacturer's protocol.
798
799 **Mass spectrometry:** Recombinant His-tagged Endocan (R&D) was immobilized on 50 µl of
800 HisPur Ni-NTA Magnetic Beads (Thermo Fisher Scientific) according to the manufacturer's
801 protocol. The beads were washed 3 times with PBS and incubated with the fraction of plasma
802 membrane proteins that were isolated from g1079 cells as described previously[60] and solubilized
803 in lysis buffer (50 mM Tris-HCl, 150 mM NaCl, 1% Triton X100, 0.1% sodium deoxycholate,
804 protease inhibitor cocktail, pH 7.5). Next, beads were washed once with lysis buffer and 3 times
805 with PBS and bounded proteins were eluted with buffer containing 8M Urea, 2M Thiourea, 10 mM
806 Tris (pH=8). Protein concentrations were determined using the QuickStart Bradford protein assay
807 (Bio-Rad) according to the manufacturer's protocol.Eluates from immunoprecipitations were
808 subsequently incubated with 5mM DTT at RT for 40 min. Then proteins were alkylated with 10
809 mM Iodoacetamide at RT for 20 min in the dark. Alkylated samples were diluted by the addition
810 of 50 mM Ammonium Bicarbonate solution at a ratio of 1:4. Next, trypsin (0.01 µg per 1 µg of
811 protein) was added, and the samples were incubated at 37°C for 14 h. After 14 h the reaction was
812 stopped by the addition of Formic acid to the final concentration of 5%. The tryptic peptides were
813 desalted using SDB-RPS membrane (Sigma), vacuum-dried, and stored at −80°C before LC-
814 MS/MS analysis. Prior to LC-MS/MS analysis samples were redissolved in 5% ACN with 0.1%
815 TFA solution and sonicated. Proteomic analysis was performed using a Q Exactive HF mass-
816 spectrometer. Samples were loaded onto 50-cm columns packed in-house with C18 3 µM Acclaim
817 PepMap 100 (ThermoFisher), with an Ultimate 3000 Nano LC System (ThermoFisher) coupled to
818 the MS (Q Exactive HF, ThermoFisher). Peptides were loaded onto the column thermostatically
819 controlled at 40°C in buffer A (0.2% Formic acid) and eluted with a linear (120 min) gradient of 4
820 to 55% buffer B (0.1% Formic acid, 80% Acetonitrile) in A at a flow rate of 350 nl/min. Mass
821 spectrometric data were stored during automatic switching between MS1 scans and up to 15

822 MS/MS scans (topN method). The target value for MS1 scanning was set to $3 \cdot 10^6$ in the range
823 300–1200 m/z with a maximum ion injection time of 60 ms and a resolution of 60000. The
824 precursor ions were isolated at a window width of 1.4 m/z and a fixed first mass of 100,0 m/z.
825 Precursor ions were fragmented by high-energy dissociation in a C-trap with a normalized
826 collision energy of 28 eV. MS/MS scans were saved with a resolution of 15000 at 400 m/z and at
827 a value of $1 \cdot 10^5$ for target ions in the range of 200-2000 m/z with a maximum ion injection time of
828 30 ms.
829 Raw LC-MS/MS data from Q Exactive HF mass-spectrometer were converted to. mgf peaklists
830 with MSConvert (version 3). For this procedure we use the following parameters: "--mgf --filter
831 peakPicking true [1,2]". For thorough protein identification in samples from immunoprecipitations,
832 the generated peak lists were searched with MASCOT (version 2.5.1) and X! Tandem (ALANINE,
833 2017.02.01) search engines against UniProt human protein knowledgebase with the
834 concatenated reverse decoy dataset. The precursor and fragment mass tolerance were set at 20
835 ppm and 0.04 Da, respectively. Database-searching parameters included the following: tryptic
836 digestion with one possible missed cleavage, static modification for carbamidomethyl (C), and
837 dynamic/flexible modifications for oxidation (M). For X! Tandem we also selected parameters that
838 allowed a quick check for protein N-terminal residue acetylation, peptide N-terminal glutamine
839 ammonia loss, or peptide N-terminal glutamic acid water loss. Result files were submitted to
840 Scaffold 4 software (version 4.0.7) for validation and meta-analysis. We used the local false
841 discovery rate scoring algorithm with standard experiment-wide protein grouping. For the
842 evaluation of peptide and protein hits, a false discovery rate of 5% was selected for both. False
843 positive identifications were based on reverse database analysis. We also set protein annotation
844 preferences in Scaffold to highlight Swiss-Prot accessions among others in protein groups.
845
846 ***In vitro* migration experiment:** Patient-derived Glioma cells (1079, 413, 408) were used for
847 encapsulation. Approximately 600k cells per well were seeded into Aggrewell well plates
848 (Stemcell Technologies) one day prior to encapsulation. Next day, the spheroids were
849 encapsulated in hydrogels using a previously described hydrogel fabrication protocol[7]. Cell
850 migration was observed at Day 1, 3, 6 and 9 post encapsulations by acquiring phase contrast
851 images on a Zeiss Axio.Z1 Observer microscope with a Hamamatsu Orca Flash 4.0 V2 Digital
852 CMOS Camera and Zeiss ZEN 2 (Blue Edition) software.

853 **Transmission Electron microscopy:** Tissue from tumor-bearing mice were resected after
854 anesthetizing and perfused with 1X PBS. Tissues were fixed in 4% paraformaldehyde and 2%

855 glutaraldehyde. Next, the tissues were fixed with 1% Osmium tetroxide followed by dehydration
856 in different concentrations of ethanol, and resin embedding. Following the embedding, sections
857 were cut to 60-90 nm thickness, and then were counterstained with Uranyl Acetate and Lead
858 citrate for imaging and analysis. Hitachi® H-7500 electron microscope was used for imaging
859 and images were captured with NanoSprint12 AMT® camera. The outer-inner blood vessel ratio
860 was calculated based on the inner-to-outer diameter of the blood vessel wall. Previously
861 published Shape adjusted ellipse (SAE) method was used to calculate the diameters[23]. The
862 SAE approach corrects for dispersion angles. One way ANOVA followed by post hoc test was
863 performed, ***P=0.0030* (tumor bearing WT vs. *Esm1* KO) groups.

864 **ATAC sequencing and analysis:** WTD and KOD tumor cells were processed for ATAC
865 sequencing and repeated at least 2 independent times as previously described[39]. Briefly, 50,000
866 cells were washed with 50mL ice cold PBS and re-suspended in 50mL lysis buffer (10 mM Tris-
867 HCl pH 7.4, 10 mM NaCl, 3 mM $MgCl_2$, 0.2% (v/v) IGEPAL CA-630). The suspension was
868 centrifuged at 500g for 10 minutes at 4 degrees. Samples were added with 50mL trans-position
869 reaction mix of Nextera DNA library preparation kit (FC-121-1031, Illumina). DNA was amplified
870 by PCR and incubated at 37ºC for 30 minutes. MinElute Lit (Qiagen) was used to isolate DNA.
871 NextSeq 500 High Output Kit v2 (150 cycle, FC-404-2002, Illumina) was used to sequence
872 ATAC library. For analysis, alignment was carried out using the Burrows-Wheeler Aligner mem,
873 peak calling using MACS2 (with parameter setting –nomodel –shift 75), GO enrichment analysis
874 and peak annotation using HOMER and Enrich R (https://maayanlab.cloud/Enrichr/). UCSC
875 Genome Browser was used to determine whether open regions displayed H3K27Ac and
876 conserved TF binding sites. Integrated Genome viewer (IGV) was utilized to represent the
877 open/peak regions in the experiments.

878 **RNA sequencing:** cDNA were used in the library preparation using Ovation® Ultralow Library
879 Systems (NuGEN) and samples were sequenced using an Illumina HiSeq 2000 sequencer
880 (Illumina, San Diego, CA) in high output mode across 9 lanes of 50bppaired-end sequencing,
881 corresponding to 4.3 samples per lane and yielding ~45 million reads per sample. Additional QC
882 was performed after the alignmentTotal counts of read-fragments that were aligned to all the
883 candidate gene regions were derived using HTSeq program
884 (www.huber.embl.de/users/anders/HTSeq/doc/overview.html) with Human Hg38 (Dec.2014)
885 RefSeq (refFlat table) as a reference and used as a basis for the quantification of gene
886 expression. Only uniquely mapped reads were used for subsequent analyses. Differential
887 expression analysis was conducted with R-project and the Bioconductor package edgeR.

888 Statistical significance of the differential expression, expressed as Log_2 Fold Change (logFC),
889 was determined, using tag-wise dispersion estimation, at p-Value of <0.005 unless stated
890 otherwise. FPKM values were reported as a measure of relative expression units.

891 **Flow cytometry:** For CD44 staining gliomaspheres were dissociated into single cells and
892 stained with anti-CD44-APC antibody (Miltenyi Biotec) according to manufacturer's protocol. For
893 CD133 staining, gliomaspheres were dissociated into single cells and stained with anti-CD133-
894 FITC (Biolegend) according to manufacturer's protocol. For apoptosis assay, cells were stained
895 with CellEvent Caspase-3/7 Green Flow Cytometry Assay Kit (ThermoFisher Scientific)
896 according to the manufacturer's protocol. To estimate the percentages of cells in the different
897 phases of the cell cycle, propidium iodide (PI) dye (ThermoFisher Scientific) was used. Cells
898 were fixed in 70% ethanol and treated with riboneuclease as recommended by the
899 manufacturer's protocol. All samples were analyzed by Attune NxT Flow Cytometer
900 (Thermofisher Scientific) and the data were processed with FlowJo 10 software.

901 **Endocan blocking antibody experiment in HBEC-5i CM**: For Endocan blocking experiments,
902 HBEC-5i cells were grown without serum and 10ul of anti-Endocan antibody (ab103590) was
903 added to 10ml of CM. 10 ug of control rabbit IgG was added to another 10 ml of CM. CM was
904 incubated 2 hours at room temp with slow agitation followed by incubation with 100ul of ProtA/G
905 magnetic beads (Thermofisher Scientific) for 1 hour. CM was then spun at 100g for 5 minutes
906 and supernatant was carefully removed without disturbing the beads and subsequently filtered
907 through 0.22μm filter.

908 **Cell proliferation assay:** AlamarBlue reagent (Thermo Scientific) or Cell-Titer Glo (Promega)
909 was used to determine the cell number under various treatments. Briefly, cells were seeded at a
910 density of 5,000 cells per well in 96-well plates. AlamarBlue reagent was added into each well
911 and fluorescence was measured (Excitation 515-565 nm, Emission 570-610 nm) using Synergy
912 HTX multi-mode reader (BioTek). CellTiter-glo was used at 1:1 ratio and measured using a
913 luminometer plate reader. Readings were taken on Day 0 and Day 3 or Day 5 after treatment.

914 **Western blot:** The cell lysates were prepared in RIPA buffer containing 1% protease and 1%
915 phosphatase inhibitor cocktail on ice. The sample protein concentrations were determined using
916 the Bradford method. Equal amounts of protein lysates (10 μg/lane) were fractionated on a
917 NuPAGE Novex 4%–12% Bis-Tris Protein Gel (Thermo Fisher Scientific) and transferred onto a
918 PVDF membrane (Thermo Fisher Scientific). Subsequently, the membrane was blocked with

919 5% skim milk or 5% BSA for 1 hour and then incubated with the appropriate antibody at 4°C
920 overnight. Membranes were then washed with 3X with TBST buffer and incubated with
921 appropriate HRP-conjugated secondary antibodies (GE Healthcare) for 1 hour at RT. Protein
922 expression was visualized with an Amersham ECL Western Blot System (GE Healthcare Life
923 Sciences). β-Actin served as a loading control. ImageJ software (NIH) was used to analyze the
924 Western blot results.

925 **Immunohistofluorescence:** Immunohistofluorescence (IHF) staining was performed as
926 described previously[14]. Briefly, tumors embedded in paraffin blocks were deparaffinized using
927 Xylene and hydrated through 100%, 95% and 75% ethanol gradient. Antigen was retrieved
928 using DakoCytomation target retrieval solution pH 6 (Dako). Samples were then blocked with
929 serum-free protein block solution (Dako) and incubated with corresponding primary antibodies
930 at 4°C overnight. Next, slides were incubated with Alexa Flour-conjugated secondary antibody
931 for 1 hr at room temperature and mounted in Vectashield mounting medium containing DAPI
932 (Vector Laboratories). Nikon A1 Confocal microscope (Nikon) was used to capture images.

933 **γ-H2AX assay**: Chamber slides or wells were covered with laminin for 24 hours prior to cell
934 seeding. Cells were allowed to grow and acclimate with treatment conditions. At the indicated
935 times, the cells were irradiated or treated. Cells were then fixed in 4% paraformaldehyde,
936 permeabilized with 0.5% Triton-X/PBS, and stained with an anti γ-H2AX antibody (1:500) and
937 anti-rabbit conjugated Alexa 594 secondary antibody was used along with DAPI. Plates were
938 imaged using EVOS microscope and ImageJ was used to manually quantify positively stained
939 cells. At least 10-15 images were taken at 20X and in different areas per group.

940 **Immunohistochemistry:** Immunohistochemistry (IHC) staining was performed as described
941 previously[28]. Briefly, tumors embedded in paraffin blocks were deparaffinized using Xylene and
942 hydrated through 100%, 95%, and 75% gradient of ethanol. Slides were then microwaved in the
943 presence of DakoCytomation target retrieval solution pH 6 (Dako). Slides were incubated with
944 0.3% hydrogen peroxide solution in methanol for 15 minutes at room temperature to inhibit
945 internal peroxide activity. Slides were then blocked with serum-free block solution (Dako) and
946 incubated with corresponding primary antibody overnight at 4°C. Next, samples were incubated
947 with EnVision+ System-HRP labeled Polymer (Dako) and visualized with DAB peroxidase
948 substrate kit (Vector Laboratories). Images were captured using EVOS® FL inverted
949 microscope (Thermo Fisher Scientific IHC scoring was performed using a previously described

950 method. Vessel quantification for IHC images were measured using Vessel Quantify_IHC and
951 IHC profiler Plugin in ImageJ, for CD31 staining in tissues[7,61]).

952 **Lentivirus production and transduction:** Lentiviruses were produced as described before[28].
953 Briefly, HEK293FT packaging cells (Invitrogen) were co-transfected with lentiviral vectors
954 encoding shRNAs or GFP or mCherry and two packaging plasmids psPAX2 and pMD2.G.
955 Growth media was changed the following day and lentiviruses-containing supernatants were
956 harvested at 72 hr after transfection and concentrated 100-fold using Lenti-X concentrator
957 (Clontech). For infection, GBM cells were dissociated into single cells with accutase and seeded
958 on laminin coated 6 well plates at $8x10^5$ cells per well. Next day, 8µg/ml of Polybrene (EMD
959 Millipore) along with viral supernanatant were added to GBM cells. Two days after infection,
960 transduced cells were selected with 1µg/ml of puromycin (Sigma) for 3 days.

961 **Tissue Microarray:** Tissue microarray consisting of 0.6-mm cores from formalin-fixed, paraffin-
962 embedded tissue blocks were generated using patient derived glioblastoma tissue samples at
963 the Osaka City University (Cohort #3 n=38) after approval of the experimental protocol by the
964 Institutional Review Board.

965 **RNA Isolation and Quantitative Real-time PCR:** mRNA was extracted and purified using the
966 RNeasy Mini kit (Qiagen) according to the manufacturer's protocol. Nanodrop 2000
967 spectrophotometer was used to determine the concentration and quality of RNA. RNA (0.5-1µg)
968 was reverse-transcribed in cDNA using iScript Reverse Transcription Supermix (Bio-Rad) and
969 then amplified using the following cycling conditions; 95°C for 5 min, and then 50 cycles of 95°C
970 for 20 s, 60°C for 20 s and 72°C for 20 s. qRT-PCR was performed on StepOnePlus thermal
971 cycler (Thermo Scientific) with SYBR Select Master Mix (Thermo Scientific). 18s, B-actin was
972 used as an internal control.

973 **Quantification and Statistical analysis:** GraphPad Prism 10 was used for statistical tests and
974 all details can be found in figure legends. Reported experiments were conducted at least three
975 independent times unless stated otherwise. Error bars on all the graphs show Mean and
976 Standard deviation (SD). Statistical analysis was performed using using the unpaired student's
977 t-test unless mentioned otherwise in figure legends. One-way ANOVA followed by post-hoc t
978 test was used for statistical comparisons of multiple groups. Log-rank analysis was used to
979 determine the statistical significance of Kaplan-Meier survival curves. *P* values less than 0.05

980 were considered to be significant. No samples, mice or data points were excluded from the
981 analysis reported.

982 **Data availability.** All raw RNA-seq data will be available in the NCBI Gene Expression
983 Omnibus (prepared prior to publication).
984

985 **Acknowledgements**
986 We would like to express our sincere appreciation to all the patients and families, who kindly
987 allowed us to obtain their tumor samples for this study. We thank Dr. Ralf Adams (Max Planck
988 Institute for Molecular Biomedicine) for generously sharing cryopreserved *Esm1* embryos.
989 Lastly, we acknowledge the contribution by all the members in the Nakano and Kornblum
990 laboratories (past and present) for technical assistance.
991

992 **Financial support**: This work was supported by NIH grants R01NS083767, R01NS087913,
993 R01CA183991, R01CA201402 (I.N.), R01NS104339 (A.B.H), NS052563 (H.I.K.) the UCLA
994 SPORE in Brain Cancer, P50 CA211015 (H.I.K.); and the Dr. Miriam and Sheldon G. Adelson
995 Medical Research Foundation (H.I.K., A.L.B., S.A.G). S.B was supported by UCLA Chancellor
996 Postdoctoral Fellowship award.
997

998 **Author Contribution**:
999 Conceptualization: S.B, M.S.P, IN, H.I.K
1000 Methodology: S.B, M.S.P, N.P.B, L.A.H, A.B.H, S.K.S, S.A.G, I.N, H.I.K
1001 Formal Analysis: S.B, M.S.P, I.N, H.I.K
1002 Laboratory investigation: S.B, M.S.P, N.S, M.S.K, N.P.B, L.A.H, A.S, S.Y, Y.G, S.D.M, D.Y,
1003 J.A.O, B.T, A.L.B
1004 Bioinformatics analysis: K.S.A, R.K, Y.Q
1005 Writing – Original Draft: S.B, M.S.P, I.N, H.K
1006 Writing – Review & Editing, S.B, M.S.P, M.A.N, N.P.B, L.A.H, I.N, H.I.K
1007 Funding Acquisition: M.S.P, K.S.A, A.B.H, L.A.H, A.L.B, S.A.G, I.N, H.I.K
1008 Resources: H.I.K, A.L.B, I.N
1009 Supervision: H.I.K, I.N
1010
1011
1012

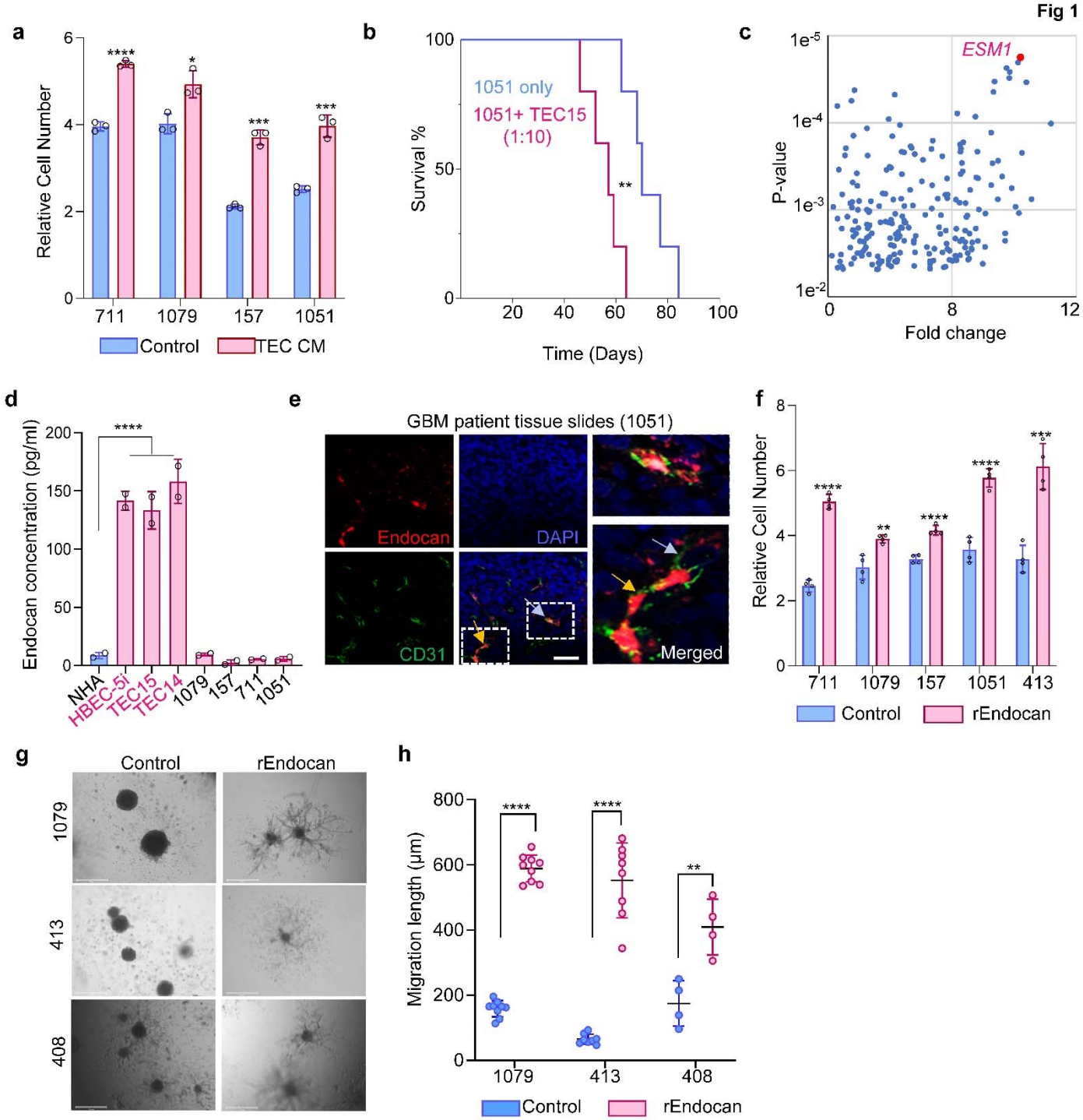

1013

1014

1015

1016

1017

1018 **Figure 1: Vascular-secreted Endocan promotes proliferation and migration of GBM cells.**
1019 **A,** Proliferation of GBM cells (711, 1079, 157, 1051) treated with control media or conditioned
1020 media collected from Tumor Endothelial Cells (TEC CM); n=3 independent experiments.
1021 *$P=0.015$, **$P=0.007$, ***$P=0.0001$, and ****$P<0.0001$.
1022 **D**, ELISA assay comparing levels of secreted Endocan in CM from Normal Human Astrocytes
1023 (NHA), Human Brain Endothelial Cells (HBEC-5i), Tumor-associated Endothelial cells (TEC15,
1024 TEC14), and GBM cells (1079, 157, 711, and 1051). One-way Anova and Tukey post-hoc test,
1025 n=2 independent experiments, ****$P<0.0001$.
1026 **E**, Representative immunofluorescence (IF) staining for Endocan (red) and CD31 (green) in
1027 formalin-fixed paraffin-embedded tissue sections from glioblastoma patient 1051. Nuclei stained
1028 with DAPI (blue). Scale bar, 50 µm.
1029 **F**, Proliferation of GBM cells (711, 1079, 157, 1051, 413) with or without rEndocan (10ng/ml).
1030 Proliferation was measured 5 days after treatment; n=4 independent experiments; **$P<0.005$,
1031 ***$P<0.0005$, ****$P<0.0001$.
1032 **G**, Representative microscopic images of control and rEndocan treated (10ng/ml) GBM
1033 spheroids encapsulated in the hydrogel. Images were taken 3 days post encapsulation. n=6
1034 spheroids per group. Scale bar, 500µm.
1035 **H,** Quantification of migration distance in control and rEndocan spheroids formed by 408, 413 or
1036 1079 cells. Data from n= 4-10 spheroids were used for analysis. **P=0.0053; ****P<0.0001. All
1037 quantitative data are average ±SD, unpaired two-tailed Student's t test was used to determine
1038 the significance of differences between the indicated groups where applicable.
1039
1040
1041
1042
1043
1044
1045
1046
1047
1048
1049
1050
1051

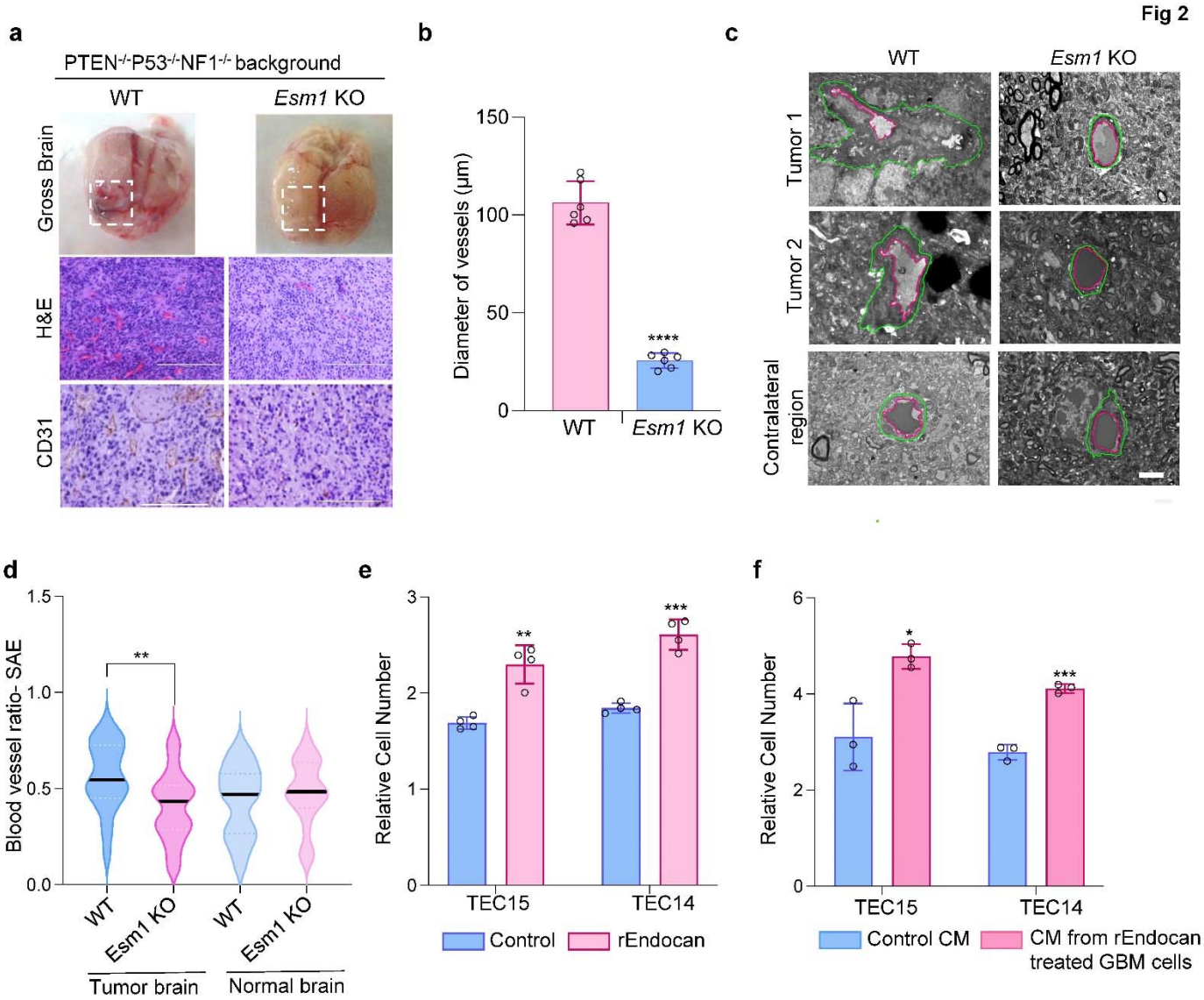

1052
1053
1054
1055
1056
1057
1058
1059
1060
1061
1062

Figure 2: Endocan is essential for establishing the hypervascular phenotype of GBM.

A, Images of the brains collected from 7080 glioma-bearing *Esm*1 WT or *Esm1* KO mice (upper panel). H&E staining of the tumor slices (middle panel, Scale bar, 200 μm) and CD31 staining of the tumor slices (lower panel, Scale bar, 200 μm).

B, Quantitation of the diameter of the blood vessels formed in tumors from *PTEN/P53/NF1* deleted glioblastoma model. CD31 positive VE cells were imaged and then measured in ImageJ using ImageJ vessel analysis tool. n=5 mice per group, ****P<0.0001.*

C, Representative transmission electron microscopy images of tumors formed in *Esm1* WT and KO mice (middle panel) and contralateral tissue region from non-tumor hemisphere (lower panel). Green and magenta lines indicate the outer and inner diameter of the blood vessels respectively. Scale bar, 2μm.

D, Measurement of the thickness of blood vessels in the tumor-bearing hemisphere of mice brains and contralateral region using Blood vessel ratio-SAE. Quantifications were performed in n=24 (WT), n=56 (KO), n=29 (normal brain WT) and n=44 (normal brain Esm1 KO). One way ANOVA followed by post hoc test, ***P=0.0030*.

E, Proliferation of rEndocan treated (10ng/ml) and untreated TEC cells (TEC 15 and TEC15). Proliferation was measured on Day 5 post treatment, ***P=0.0012, ****P=0.0013*.

F, Proliferation of TEC15 and TEC14 cells treated with conditioned media collected from the control GBM cells or GBM cells pretreated with rEndocan (10ng/ml) for 3 days. Proliferation was measured on day 5 post treatment. **P=0.0173, ****P<0.0002*. All quantitative data are average ±SD.

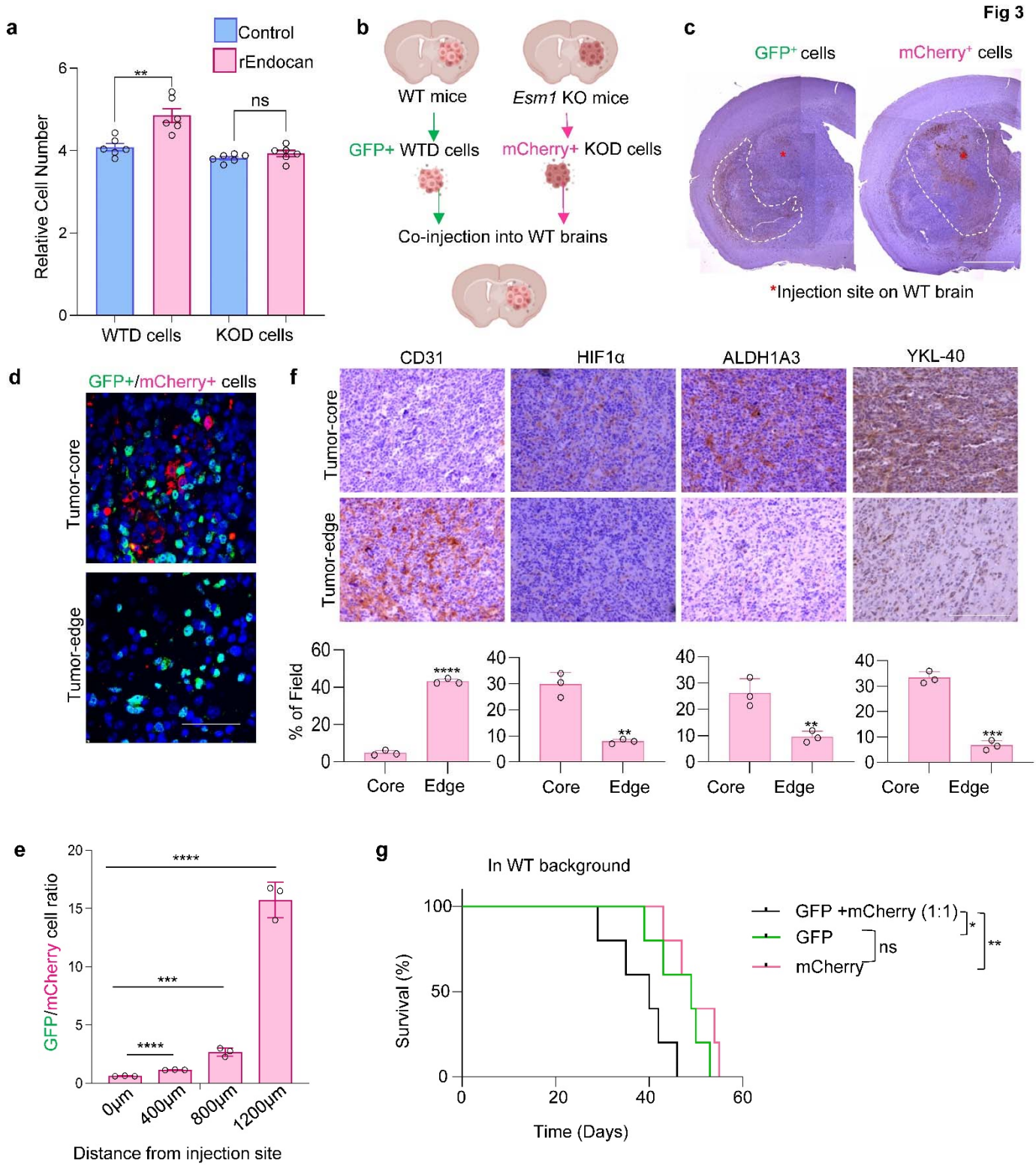
Fig 3
a
Control
rEndocan
Relative Cell Number
**
ns
WTD cells
KOD cells
b
WT mice
Esm1 KO mice
GFP+ WTD cells
mCherry+ KOD cells
Co-injection into WT brains
c
GFP+ cells
mCherry+ cells
*Injection site on WT brain
d
GFP+/mCherry+ cells
Tumor-core
Tumor-edge
f
CD31
HIF1α
ALDH1A3
YKL-40
Tumor-core
Tumor-edge
% of Field
Core
Edge
e
GFP/mCherry cell ratio
0μm
400μm
800μm
1200μm
Distance from injection site
g
In WT background
Survival (%)
Time (Days)
GFP +mCherry (1:1)
GFP
mCherry
ns

1096

1097

Figure 3: Endocan induces stable phenotypic alterations of GBM cells regulating their spatial identity.

A, Proliferation assay of control and rEndocan treated (10ng/ml) WTD and KOD cells. ***P=0.0023*, n=3 independent experiments.

B, Schematic figure delineating the steps for the experiment. Briefly, mouse 7080 spheres were implanted into brains of WT and *Esm1* KO host, once tumors were formed, they were isolated into single cells, and were followed by labeling *Esm1* KO derived spheres with mCherry and WT derived spheres with GFP. Cells were then co-injected into WT host (n=5 mice).

C, Representative IHC staining with anti-GFP (left) and anti-mCherry (right) antibodies of mice brains co-injected with WTD (GFP^+) and KOD ($mCherry^+$) cells (n=5 mice). The boundaries of the staining areas are shown by white lines, injection site indicated by red asterisk. Scale bar, 2mm.

D, Representative IHF images of mice brain sections stained with anti-GFP (green), anti-mCherry (red) antibodies and DAPI (blue). Scale bar, 50 μm

E, Ratio of GFP+ and mCherry+ cells in IHF images as in “D” at different distances from the site of injection. Quantification was performed using ImageJ software where mCherry+ cells and GFP+ cells were divided by DAPI staining. n=3 mice. ****P<0.0001*; 800μm vs. 0μm, ****P=0.0006*; 1200μm vs. 0μm, ****P<0.0001*.

F, Representative IHC images of core (upper panel) and edge regions (middle panel) of the tumor obtained as in “D” stained for CD31, HIF1α, ALDH1A3, and YKL-40. % of field positive areas for indicated proteins on lower panel (n=5 independent mouse samples). ***P<0.01*, ****P=0.0001*, ****P<0. 0001.Scale* bar, 200μm.

G, Kaplan-Meier survival analysis of *Esm1* WT mice intracranially injected with WTD and KOD cells or the mixture of both at 1:1 ratio. (n=5 mice per group), **P*=0.047; ns. - non significant (*P*=0.31); ***P*=0.00642. *P*-values were determined by log-rank test. All quantitative data are average ±SD.

Fig 4

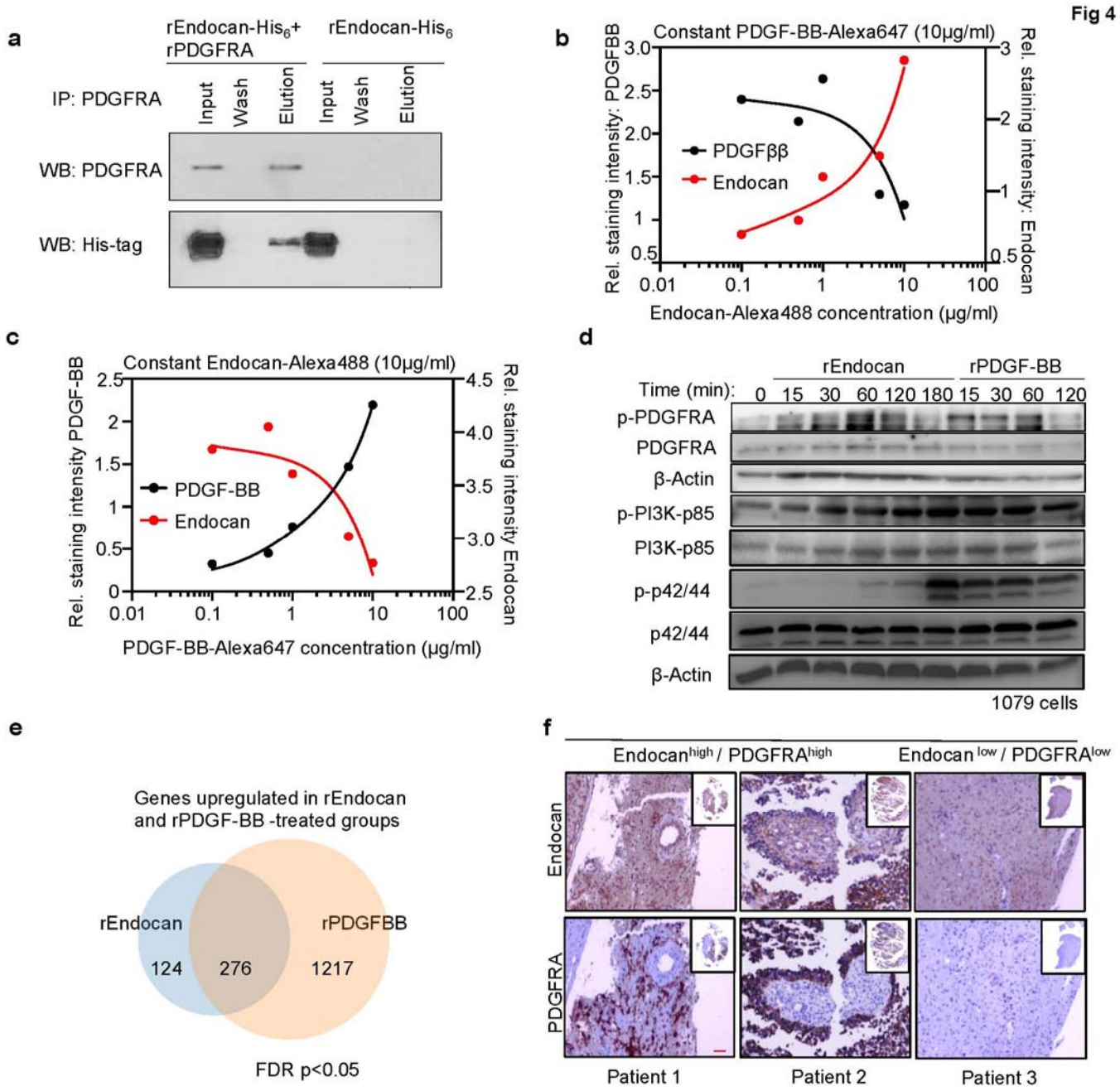

1131

1132

1133

1134

1135

1136

1137

1138

1139 **Figure 4: Endocan binds to and activates PDGFRA in human glioblastoma cells.**
1140 **A,** Western blot (WB) analysis of samples obtained during pull down assay of His-tagged
1141 rEndocan and Fc-tagged rPDGFRA.
1142 **B, C** Competition binding assay of Endocan-Alexaflour488 and PDGF-BB-Alexaflour647. 1079
1143 cells were incubated with indicated concentrations of both proteins and subsequently analyzed
1144 by FACS.
1145 **D**, WB analysis of 1079 cells incubated with 10ng/ml rEndocan or rPDGF-BB for the indicated
1146 period of time.
1147 **E,** Venn diagram showing genes which expression was altered by rEndocan, and rPDGF-BB
1148 after 3 days incubation as determined by RNAseq analysis in 413 cells.
1149 **F**, Representative immunohistochemical (IHC) images showing staining for Endocan (top panel)
1150 and PDGFRA (bottom panel) in three glioblastoma patients (Tissue Micro Array set generated
1151 from Osaka university cohort) Scale bar, 100μm. All quantitative data are average ±SD.
1152
1153
1154
1155
1156
1157
1158
1159
1160
1161
1162
1163
1164
1165
1166
1167
1168
1169
1170

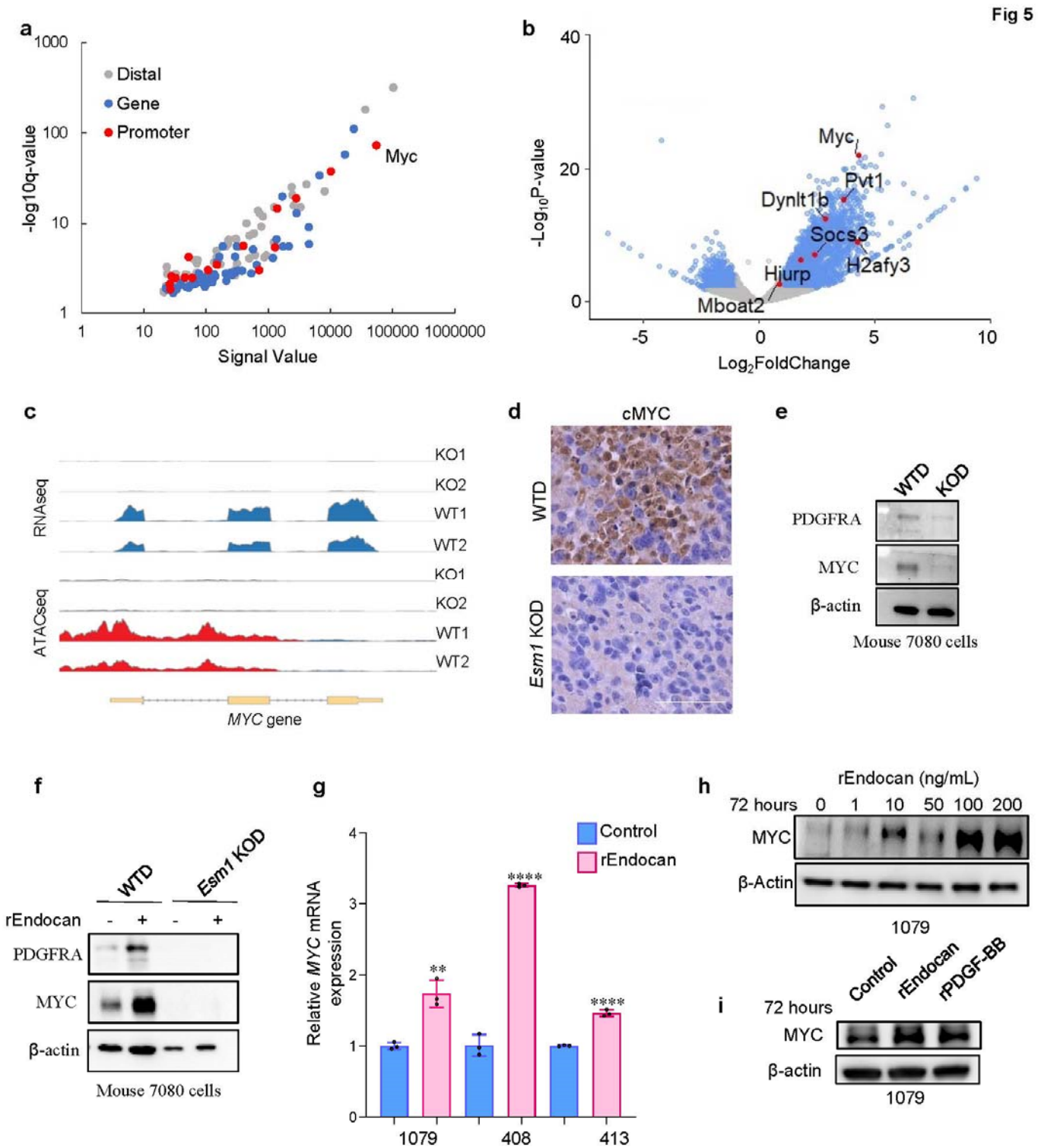

1171

1172

1173

Figure 5: Endocan induces changes in the chromatin structure in the *Myc* promoter region.

A, ATAC-seq analysis of tumors derived from *Esm1* WT and KO mice (n=2 mice per group). Individual dots represent peaks located in gene promoter region (red), in transcribed sequence (blue) and outside of the gene (gray). P-value of differences between *Esm1* WT and KO samples is indicated as well as normalized signal intensity.

B, Volcano plot showing differentially expressed genes between tumors derived from *Esm1* WT and KO mice as determined by RNAseq analysis. (n=3 mice per group). Genes with altered chromatin structure of their promoter region as determined by ATAC-seq analysis are indicated with red dots.

C, Sequencing read coverage of *Myc* gene as determined by RNA-seq (gene expression; blue) and ATAC-seq (chromatin accessibility; red) of the tumors as in "A" (n=2 mice per group).

D, Representative microscopic images of WTD and KOD tumor slides stained with anti-MYC antibody. Scale bar, 100μm.

E, Western blot analysis of WTD and KOD cells.

F, Western blot analysis of WTD and KOD cells treated or untreated with rEndocan (10ng/ml) for 3 days.

G, qRT-PCR analysis of *MYC* expression in control and rEndocan treated cells human GBM cells (1079, 408 and 413 cell lines). ***P=0.003*, ****P<0.0001*, n=3 independent experiments.

H, Western blot analysis for MYC and β- actin protein in 1079 cells treated with increasing doses of rEndocan for 72 hours.

I, Western blot analysis for MYC and β- actin protein in 1079 cells treated with rEndocan and rPDGF-BB for 72 hours. All quantitative data are average ±SD.

Fig 6

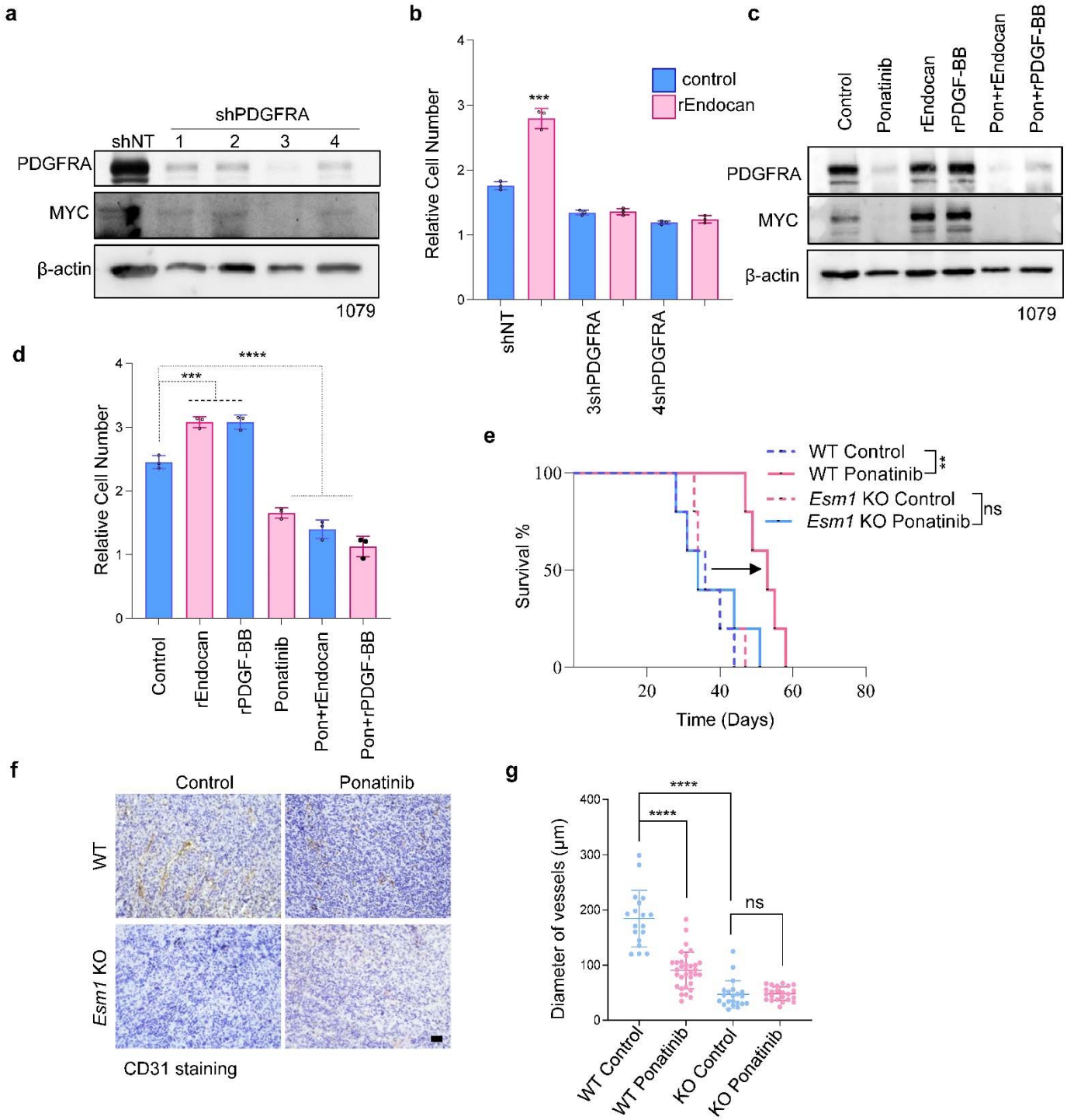

1208

1209

1210

1211

Figure 6: Inhibition of PDGFRA pathway attenuates effect of endocan on GBM cells.

A, Western blot analysis of 1079 GBM cells after lentiviral mediated knockdown of PDGFRA with 4 different shRNAs against PDGFRA or Non Target shRNA (NT) as a control.

B, Effect of rEndocan on proliferation of 1079 cells infected with shNT or shPDGFRA lentiviruses. n=3 independent experiments. ****$P<0.0001$.

C, Western blot analysis of 1079 cells depicting PDGFRA, MYC, and β-actin protein level expression in cells treated with rEndocan, rPDGF-BB, ponatinib and their combinations for 72 hours.

D, Effect of ponatinib on proliferation of 1079 cells incubated with rEndocan or rPDGF-BB. n=3 biological replicates, one-way ANOVA, post hoc T test. ***$P=0.0001$, ****$P<0.0001$.

E, Kaplan Meier survival analysis of Bl/6 mice intracranially injected with WTD and KOD cells and treated with 50mg/kg/day dose of ponatinib for 5 days using oral-gavage. n=5 mice per group, *P*-value was determined by log-rank test; WT control vs. WT ponatinib, **$P=0.00184$; KO control vs. KO ponatinib, *P=0.87, not significant.*

F, Representative microscopic images of immunohistochemical (IHC) staining with anti-CD31 antibody of tumor sections obtained from mice as in “E”.

G, Blood vessels density from tumor sections stained with CD31 antibody was analyzed using ImageJ software (n=20-33 vessels/group). Quantitative data are average ±SD; ****$P<0.0001$; *P=0.7852,* not significant. Scale bar, 100μm. All quantitative data are average ±SD.

1

Fig 7

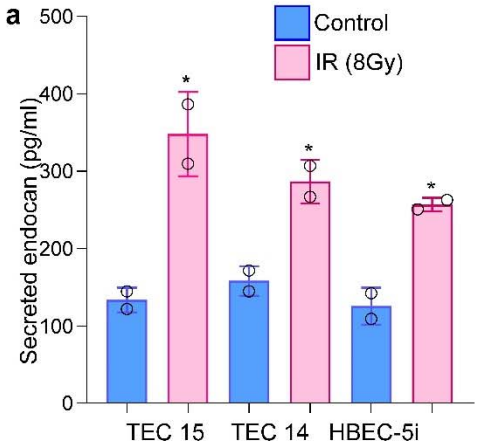

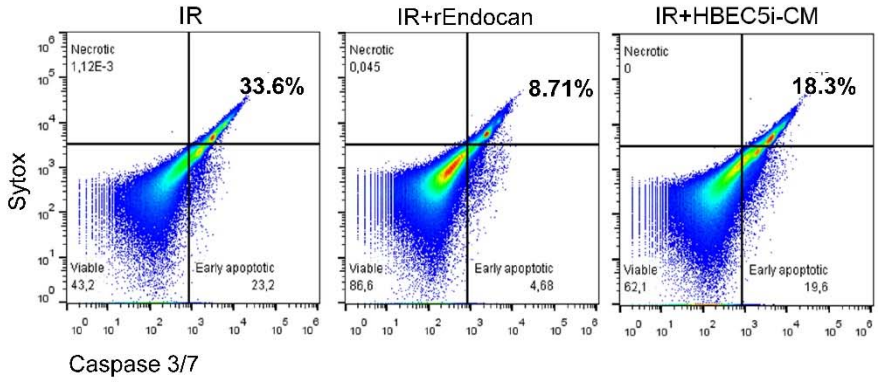

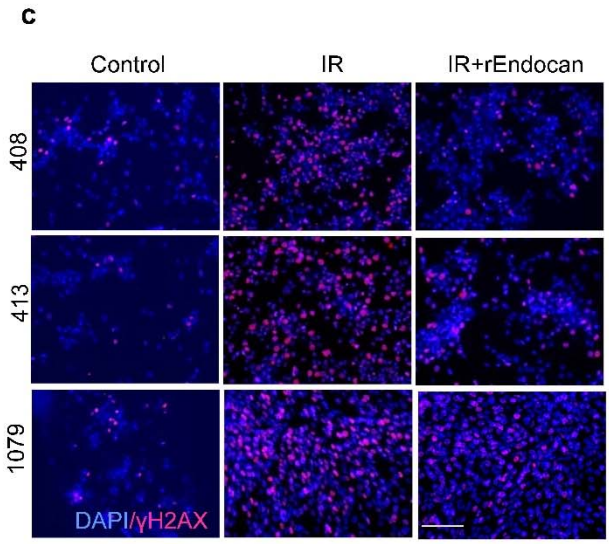

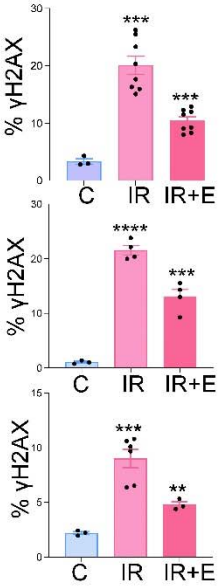

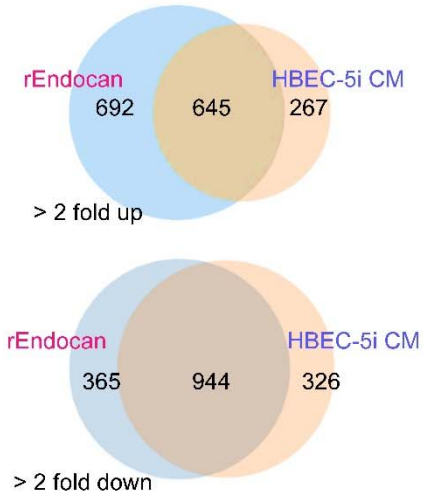

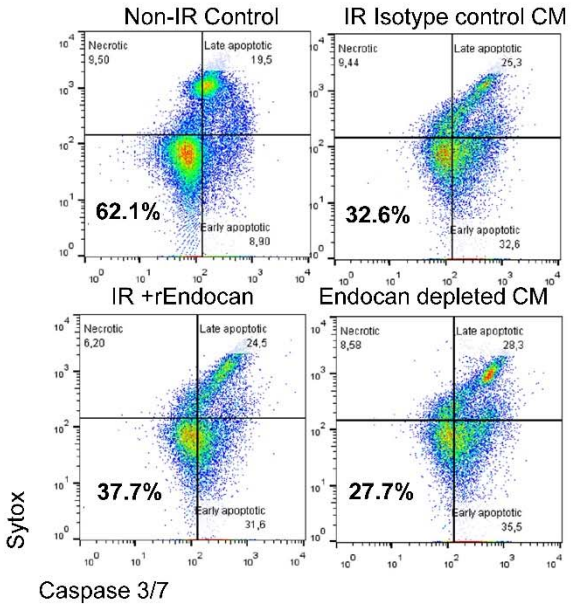

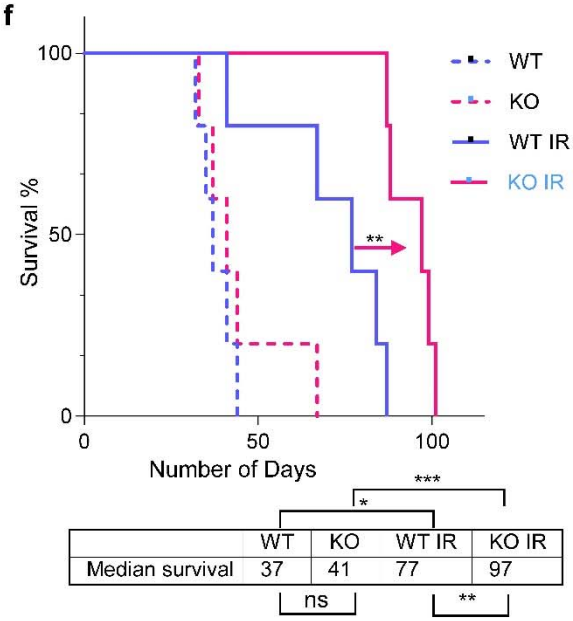

	WT	KO	WT IR	KO IR
Median survival	37	41	77	97

Figure 7: Endocan protects glioblastoma cells from radiotherapy.

A, ELISA assay comparing levels of secreted Endocan in conditioned media collected from HBEC-5i cells, TEC14, and TEC15 cells following irradiation with 8 Gy at 48-hour post radiation time-point. n=2 independent experiments. **P=0.018, **P=0.0332*; ****P=0. 0333.*

B, Flow cytometry analysis of 711 cells treated with rEndocan or HBEC-5i CM and for 3 days and subsequently irradiated with 8 Gy. Samples were collected on Day 5 after irradiation and stained for caspase 3/7 and SYTOX.

C, Representative microscopic images of GBM cells (408, 413, 1079) treated with rEndocan for 3 days and then treated with 8 Gy. Sham irradiated cells were used as control. Cells were fixed 16 hours after radiation and stained for γ-H2AX (Ser139) (left panel). Images were taken from multiple regions and n=3 independent replicates. % γH2AX positive cells were measured by dividing γH2AX cells by a total number of nuclei (DAPI positive cells) using ImageJ software (right panel). Scalebar: 125μm. ***P=0.0012*, ****P<0.001*, and *****P<0.0001*.

D, FACS analysis of Caspase 3/7 and SYTOX staining in 1051 GBM cell preincubated for 3 days with HBEC-5i CM that was incubated with Endocan blocking antibody (Endocan depleted CM), or isotype control antibody; cells preincubated with rEndocan was used as a positive control. After incubation cells were irradiated at 8 Gy and analyzed after 2 more days.

E, Venn diagram representing differentially expressed genes in 1051 GBM cells irradiated with 8 Gy alone (control) or in a presence of rEndocan or CM from HBEC5i cells. Cells were collected 5 days after radiation. Genes which expression was altered at least 2 folds were used for the analysis.

F, Kaplan Meier survival analysis of *Esm1* WT or *Esm1* KO mice intracranially injected with 7080 cells and subsequently irradiated with 3 doses of 2.5 Gy 14 days after injection. n=5 mice per group. *P*-value was determined by log-rank test, *ns – non significant*; **P=0.00875; **P=0.00443*; ****P=0.00206*. All quantitative data are average ±SD.

Fig 8

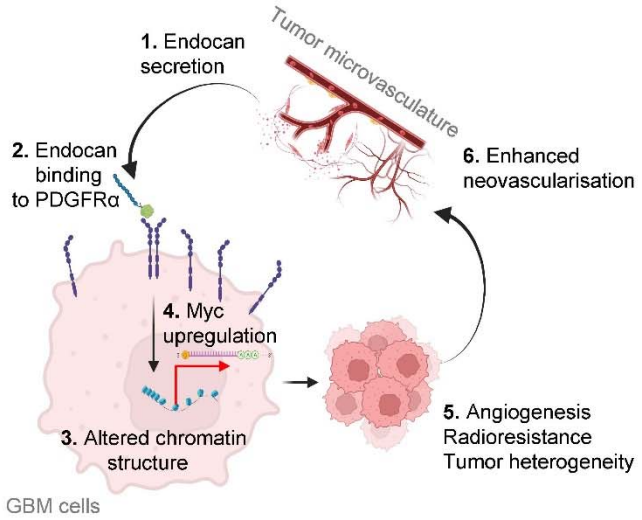

Figure 8: Schematic summary illustrating the role of Endocan in GBM-VE crosstalk. Endocan secreted by VE cells binds to PDGFRA receptor and activates downstream pathway, resulting in upregulated MYC expression and subsequent increase in GBM proliferation, radioresistance, intratumoral heterogeneity and further enhancement of angiogenesis.

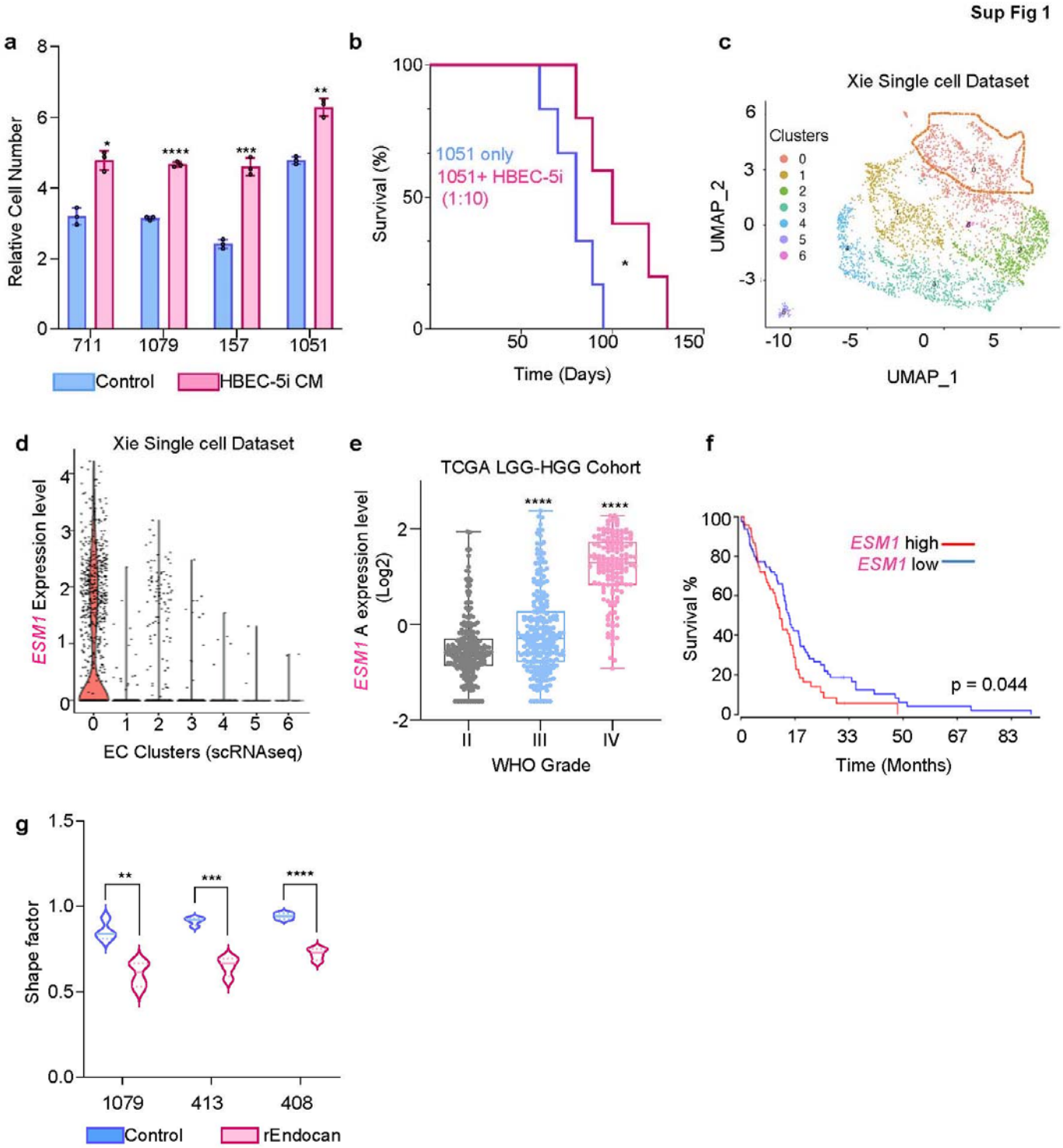
Sup Fig 1
a
Relative Cell Number
711
1079
157
1051
Control
HBEC-5i CM
b
Survival (%)
1051 only
1051+ HBEC-5i
(1:10)
Time (Days)
c
Xie Single cell Dataset
Clusters
UMAP_2
UMAP_1
d
Xie Single cell Dataset
ESM1 Expression level
EC Clusters (scRNAseq)
e
TCGA LGG-HGG Cohort
ESM1 A expression level (Log2)
WHO Grade
f
ESM1 high
ESM1 low
Survival %
p = 0.044
Time (Months)
g
Shape factor
1079
413
408
Control
rEndocan

Supplementary Figure 1:

A, Proliferation of GBM cells (711, 1079, 157, 1051) treated with control media or conditioned media collected from Human Brain Endothelial Cells-5i (HBEC-5i) cells; n=3 independent experiments. *$P=0.0017$, **$P=0.0007$, ***$P=0.0002$, and ****$P<0.0001$.

B, Kaplan-Meier survival analysis of SCID mice intracranially injected with gliomaspheres alone (1051) or gliomaspheres with VE cells (1051+HBEC-5i) at a 10:1 ratio. (n=5 mice per group). Log-rank test, *$P=0.0323$.

C, Analysis of Xie single cell RNAseq dataset[15] showing different clusters of VE cells present within the GBM tumor. Cells related to cluster 0 are highlighted.

D, Analysis of *ESM1* expression in clusters shown in "C".

E, Expression of *ESM1* in TCGA's WHO grade II, III, and IV glioma tumors. One-way ANOVA followed by Tukey's post hoc test; ****$P<0.0001$.

F, Kaplan-Meier analysis showing the survival of 667 glioma patients subdivided based on *ESM1* expression level. Log-rank test; *$P = 0.044$.

G, Quantification of shape factor/circularity in rEndocan treated and control group of spheroids formed by 408, 413 or 1079 cells. Circularity was calculated using ImageJ shape description. n=24 spheroids for independent experiments, **P=0.0016; ***P=0.0001; ****P<0.0001. All quantitative data are average ±SD.

Sup Fig 2

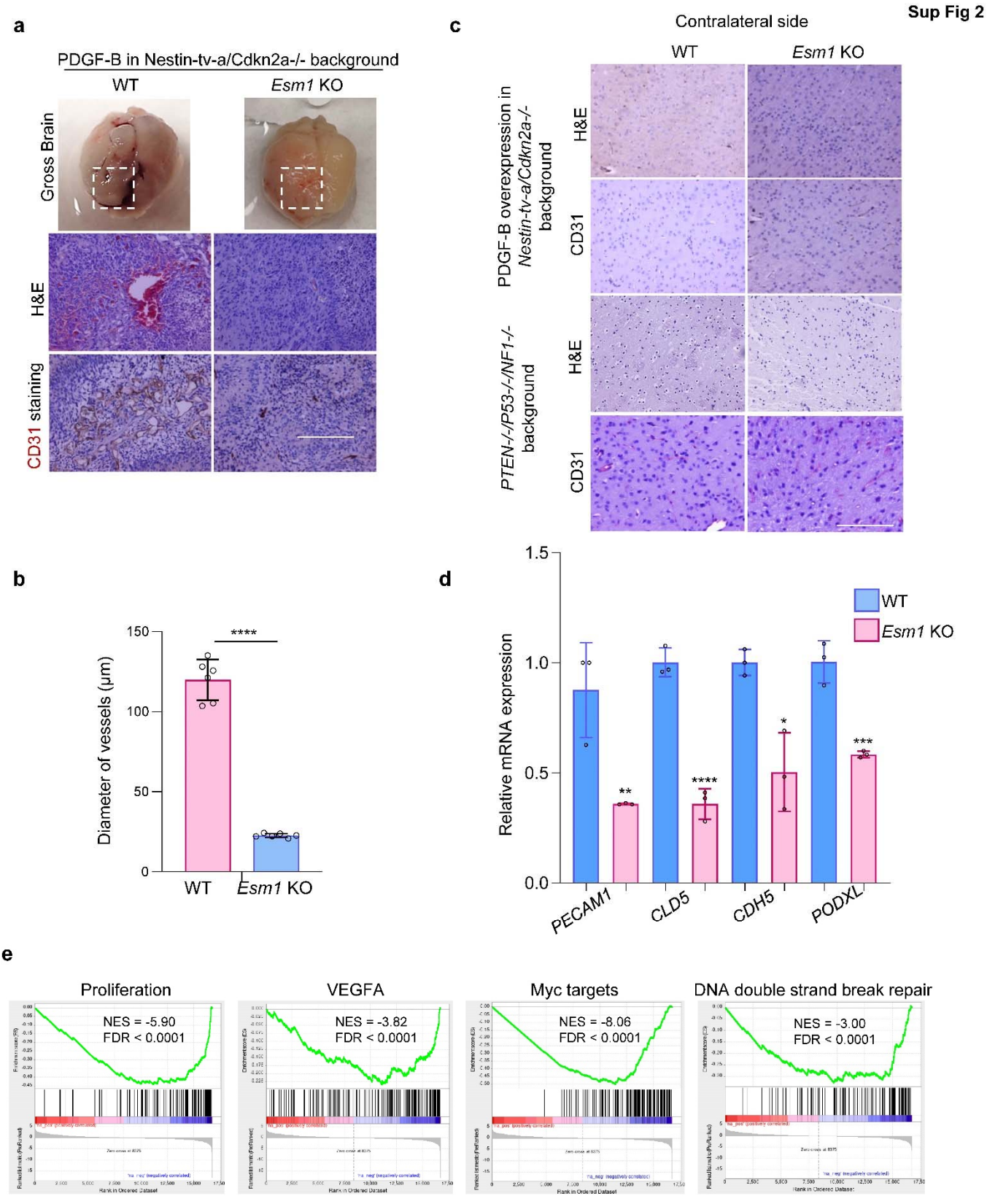

1341

Supplementary Figure 2:

A, Tumors formed by murine glioblastoma cells (isolated from Nestin-Tva/Cdkn2a-/- mice intracranially injected with RCAS-PDGFB lentiviruses) in WT and *Esm*1 KO mice brains. Images of the brains (upper panel); H&E staining of the tumor slices (middle panel, Scale bar, 200 μm); CD31 staining (lower panel, Scale bar, 200 μm).

B, Quantitation of the diameter of the blood vessels in samples as in "A". n=5 mice brains, *****P<0.0001.*

C, H&E staining (upper panel) and CD31 staining (lower panel) of non-tumor/contralateral brain sections obtained from tumor bearing *Esm1* WT and KO mice injected with cells related to two different mouse GBM models. Scale bar, 200 μm.

D, qRT-PCR analysis of expression of vascular markers genes (*Pecam1, Cld5, Cdh5, Podxl*) from tumors formed in WT and *Esm1* KO mice. n=3 replicates; **P=0.0101; **P=0.0141; ***P=0.0017; ****P=0.0003.*

E, Gene Set Enrichment Analysis (GSEA) plots comparing gene expression in tumors formed in *Esm1* KO vs. WT mice. All quantitative data are average ±SD.

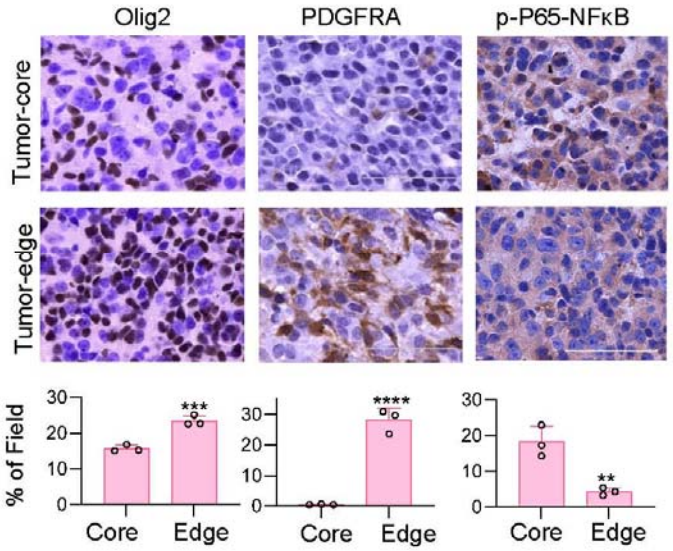

1374

1375 **Supplementary Figure 3:**

1376 Representative IHC images of core and edge regions of the tumors obtained as in "Fig 3D" and
1377 stained for PDGFRA, Olig2 and anti-pP65-NF-κB (upper panel). % of field positive areas for the
1378 indicated proteins (lower panel). Samples from n=5 mice. ***P=0.0062*, ****P=0.0015*, *****P=0.*
1379 *0003.Scale* bar, 200μm. All quantitative data are average ±SD.

1380
1381
1382
1383
1384
1385
1386
1387
1388
1389
1390
1391
1392
1393
1394
1395

Sup Fig 4

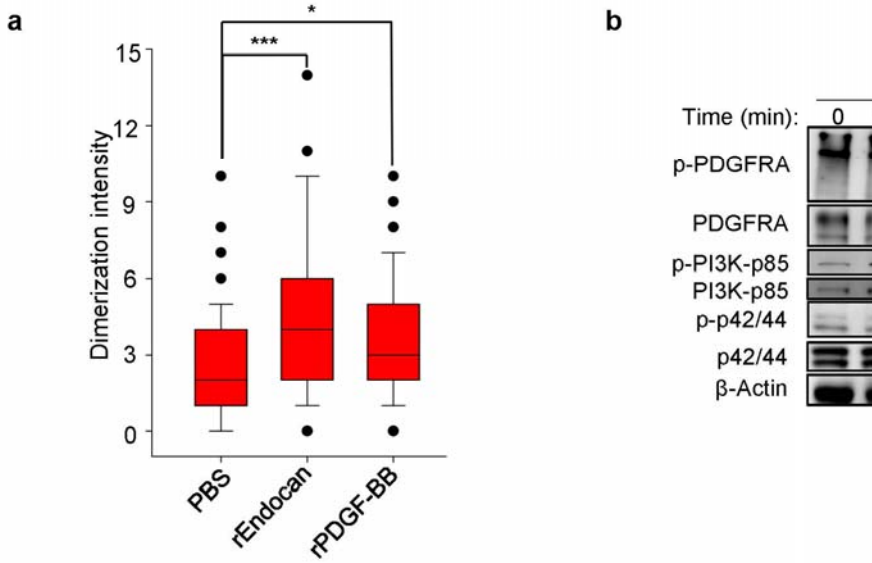

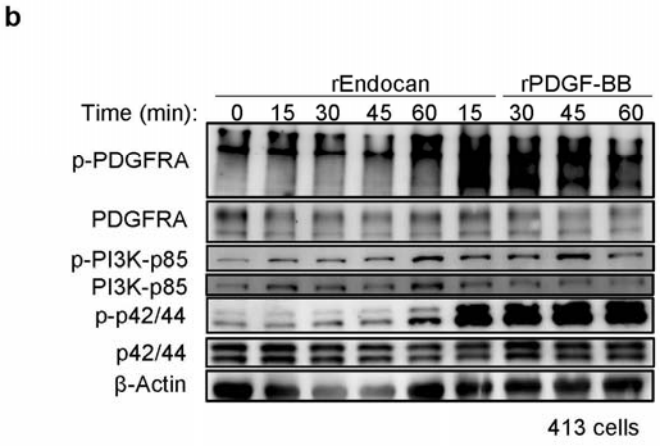

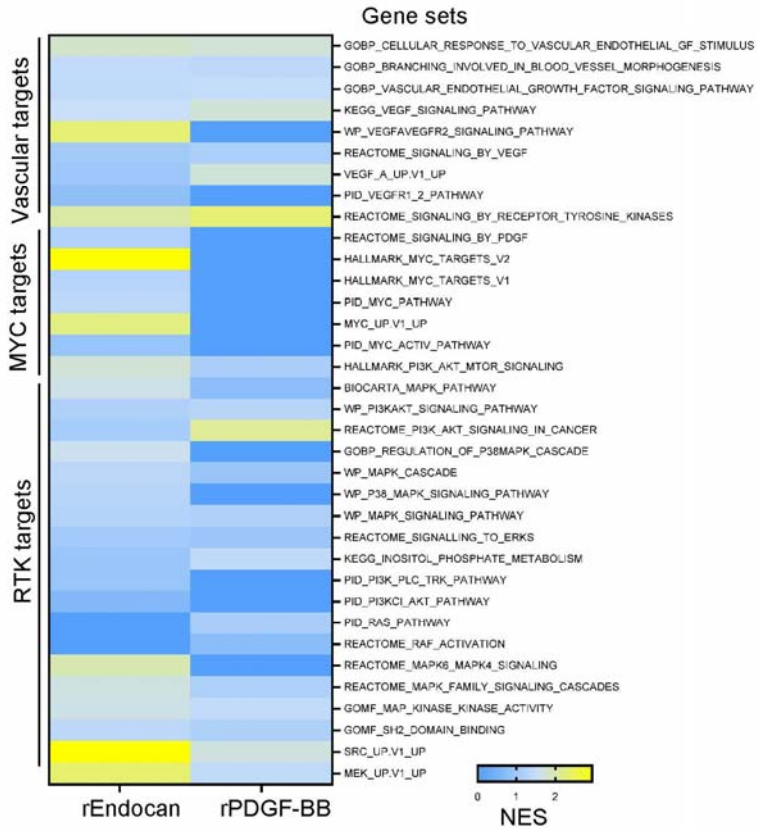

1396

1397

1398

1399

1400 **Supplementary Figure 4**

1401 **A,** PDGFRA dimerization intensity determined by *In situ* Proximity Ligation assay (PLA) in 157
1402 cells treated with rEndocan, rPDGF-BB or PBS (negative control). *P<0.05, ***P<0.001.

1403 **B**, Western blot analysis of 413 cells incubated with 10ng/ml rEndocan or rPDGFBB for the
1404 indicated periods of time.

1405 **C,** Heatmap showing normalized enrichment scores (NES) calculated from RNAseq data of 413
1406 cells treated with 10ng/ml rEndocan or rPDGF-BB for 48 hours, n=3 biological replicates.

1407
1408
1409
1410
1411
1412
1413
1414
1415
1416
1417
1418
1419
1420
1421
1422
1423
1424
1425
1426
1427
1428
1429
1430
1431
1432
1433

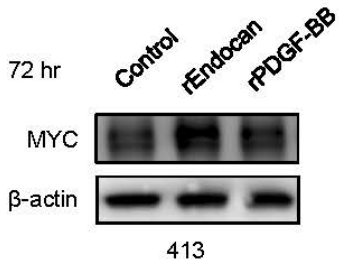

1434

1435 **Supplementary Figure 5:**

1436 Western blot analysis of 413 cells treated with 10ng/ml rEndocan and rPDGF-BB for 72 hours.

1437

1438

1439

1440

1441

1442

1443

1444

1445

1446

1447

1448

1449

1450

1451

1452

1453

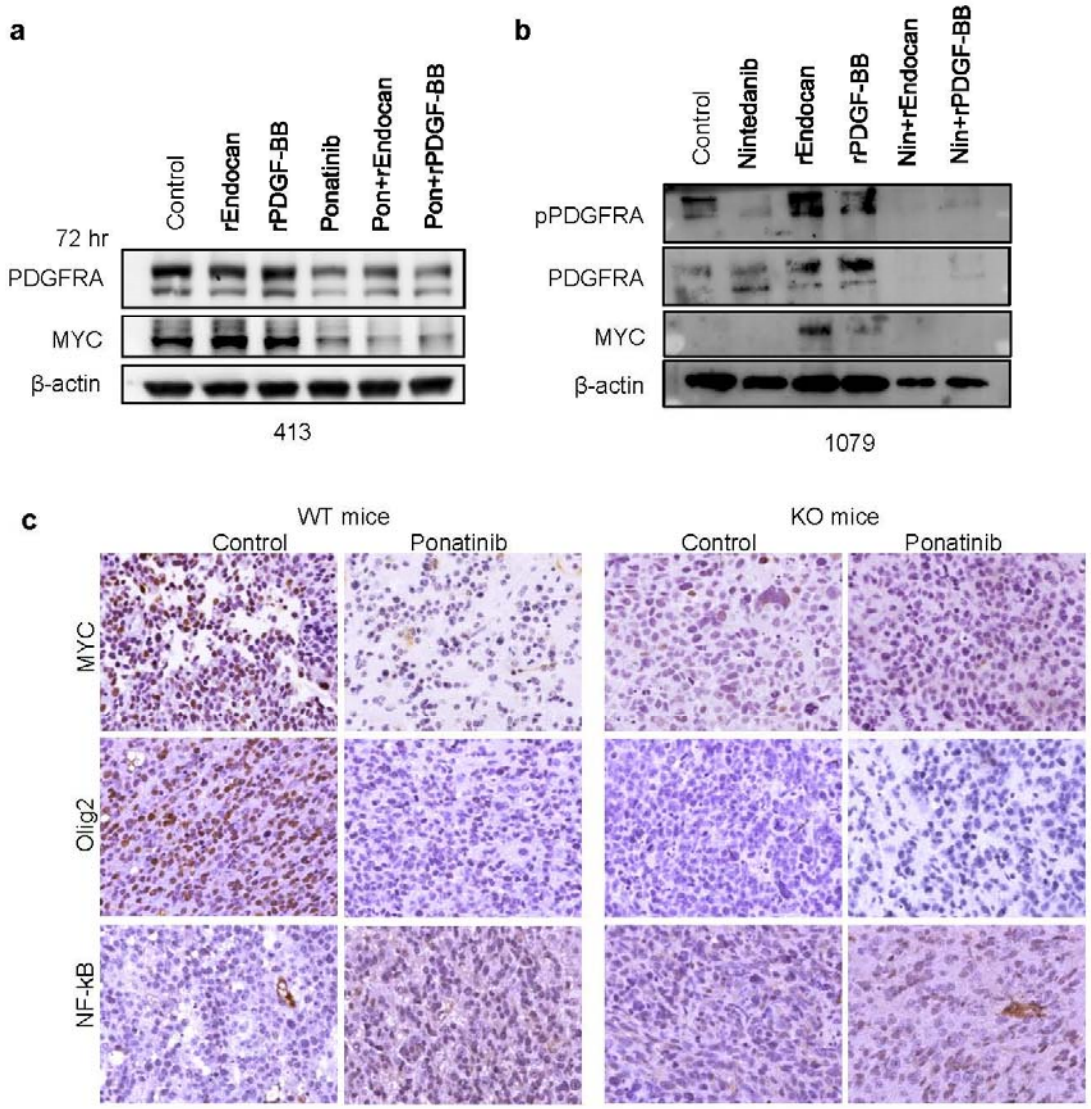

Supplementary Figure 6:

A, Western blot analysis of 413 cells treated with rEndocan, rPDGF-BB, ponatinib (Pon) and their combination treatment for 72 hours.

B, Western blot analysis of 1079 cells treated with rEndocan, rPDGF-BB, Nintedanib and their combination treatment for 72 hours.

C, Representative IHC staining for MYC, Olig2, and P65-NF-κB of tumors formed by 7080 cells in *Esm1* WT or KO mice that were treated with ponatinib or the solvent. Scale bar, 100μm.

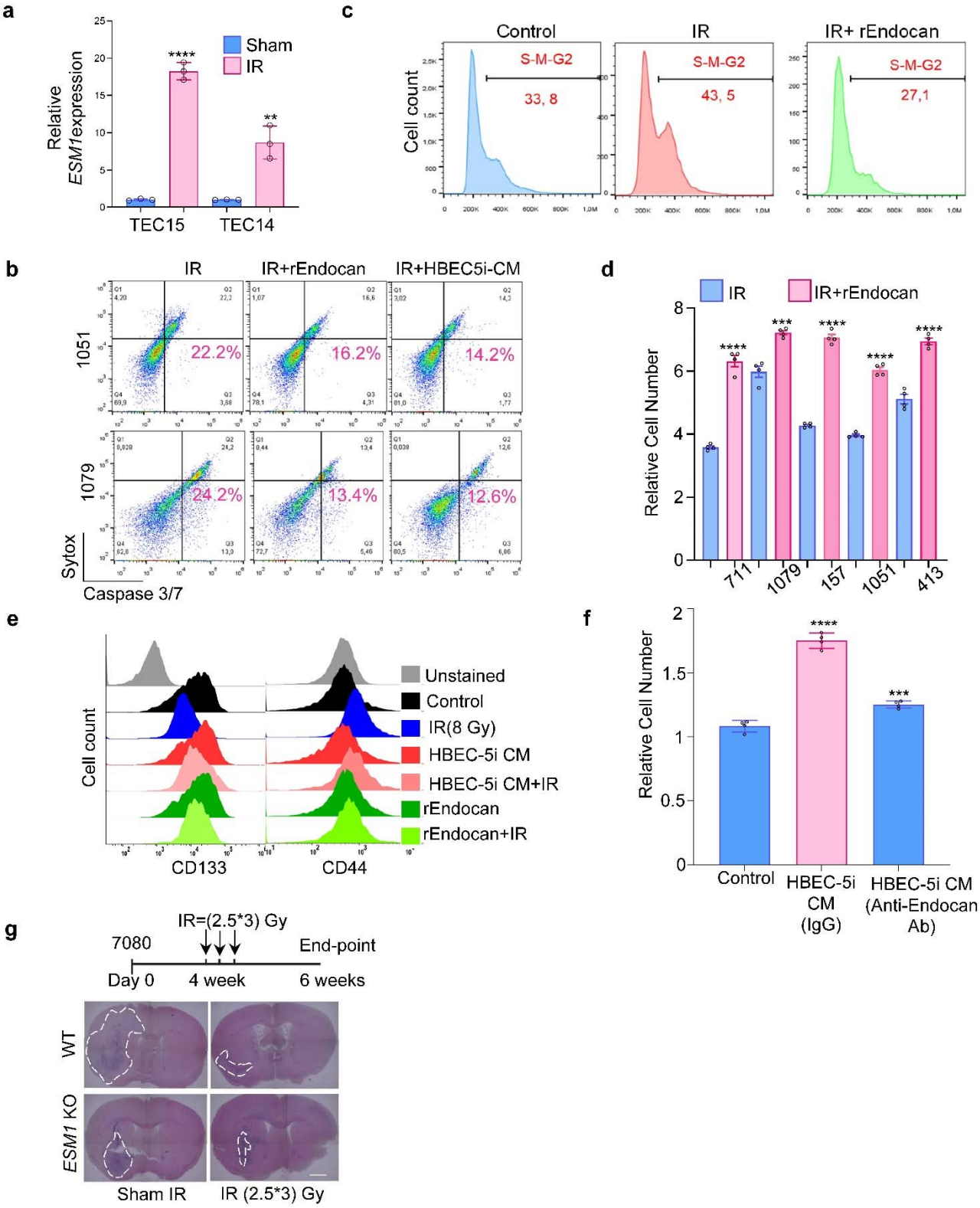
a
Relative ESM1expression
Sham
IR
****
**
TEC15
TEC14
c
Control
IR
IR+ rEndocan
Cell count
S-M-G2
33, 8
43, 5
27,1
b
IR
IR+rEndocan
IR+HBEC5i-CM
1051
1079
22.2%
16.2%
14.2%
24.2%
13.4%
12.6%
Sytox
Caspase 3/7
d
IR
IR+rEndocan
Relative Cell Number
711
1079
157
1051
413
e
Unstained
Control
IR(8 Gy)
HBEC-5i CM
HBEC-5i CM+IR
rEndocan
rEndocan+IR
Cell count
CD133
CD44
f
Relative Cell Number
Control
HBEC-5i CM (IgG)
HBEC-5i CM (Anti-Endocan Ab)
g
IR=(2.5*3) Gy
7080
End-point
Day 0
4 week
6 weeks
WT
ESM1 KO
Sham IR
IR (2.5*3) Gy

1464

1465

Supplementary Figure 7:

A, qRT-PCR analysis of *ESM1* gene expression in TEC15 and TEC14 VE cells 48 hours after treatment with 8 Gy radiation; n=3 independent experiments, **P=0.0039; ****P<0.0001*.

B, FACS analysis of caspase 3/7 and SYTOX staining of 1051 cells that were preincubated with rEndocan or HBEC-5i CM for 3 days, irradiated with 8 Gy and stained two days later.

C, FACS analysis of cell cycle distribution of 1051 cells that were left untreated, irradiated with 8Gy or preincubated for 3 days with rEndocan and subsequently irradiated.

D, *In vitro* radio-sensitivity assay of gliomaspheres (711, 1079, 157, 1051, and 413) pretreated with rEndocan for 3 days and irradiated with 8Gy. Cell growth was measured on day 5 after irradiation. n=4 independent experiments.

E, FACS analysis of CD133 and CD44 staining of 1079 cells pretreated with rEndocan or HBEC-5i CM for 3 days, irradiating with 8Gy and stained two days later. Unstained cells were used as control. ****P<0.001, ****P<0.0001*.

F, *In vitro* radio-sensitivity assay of 1079 cells preincubated for 3 days with control media, or HBEC-5i CM that was incubated with Endocan blocking antibody (Endocan depleted CM), or isotype control antibody. After incubation cells were irradiated at 8 Gy and analyzed after 3 more days. n=4 independent experiments. ****P=0.0008, ****P<0.0001*.

G, Representative H&E images of brain sections obtained from *Esm1* WT or *Esm1* KO mice intracranially injected with 7080 cells and subsequently irradiated with 3 doses of 2.5 Gy 14 days after injection. n=5 mice per group. Scale bar, 500μm. All quantitative data are average ±SD.